Diffusional homogenization of light REE in garnet from the Day Nui Con Voi Massif in N-Vietnam: Implications for Sm-Nd geochronology and timing of metamorphism in the Red River shear zone

Robert Anczkiewicz[1*], Matthew Thirlwall[2], Olivier Alard[3#], Nick W. Rogers[3], Chris Clark[4]

[1]Institute of Geological Sciences, Polish Academy of Sciences, Kraków Research Centre, Senacka 1, PL 30001 Kraków, Poland

[2]Department of Earth Sciences, Royal Holloway University of London, Egham, Surrey, TW20 0EX, UK

[3]Department of Earth and Environmental Sciences, The Open University, Walton Hall Milton Keynes MK7 6AA, UK

[4]Institute for Geoscience Research (TIGeR), Department of Applied Geology, Curtin University of Technology, GPO Box U1987, Perth, WA 6845, Australia

[#]Present address Géosciences Montpellier, UMR 5243 - CC 60, Université Montpellier 2, Place E. Bataillon , 34095 Montpellier cedex 5, France.

*Corresponding author:
Robert Anczkiewicz
Institute of Geological Sciences
Polish Academy of Sciences
Kraków Research Centre
Ul. Senacka 1
31-002 Kraków, Poland
E-mail: ndanczki@cyf-kr.edu.pl
Tel: +48 12 3705224
Fax: +48 12 4221609

Abstract

High-grade migmatitic and mylonitic gneisses from the Day Nui Con Voi massif in northern Vietnam record temperatures of 760-810 °C at pressures of 6-10 kbars. High temperature conditions have resulted in the development of major element diffusional profiles in garnet. Laser ablation ICP-MS analyses of trace elements indicate that REE and Hf closely followed Rayleigh-like fractionation trends but underwent significant post-crystallization modification. Light REE and to a lesser extent, HREE rim-to-rim zonation profiles show progressive flattening with the decreasing garnet size. Nd and Sm are completely homogenized in the crystals smaller than 1.5 mm, while Lu always preserves variable degree of core-to-rim concentration gradient. The observed REE patterns are interpreted as resulting from the combination of protracted garnet growth of progressively smaller crystals and intracrystalline diffusion. This had profound influence on Sm-Nd geochronology and resulted in isochron ages ranging from 50 to 32 Ma. The youngest age was obtained for a sample, where all garnet crystals are smaller than 2 mm and recorded light REE profiles are completely or nearly completely homogenized. Thus, only the youngest age represents geologically meaningful event, and 31.7±0.9 Ma age is interpreted as the best estimate of the resetting episode due to high-temperature diffusional homogenization of light REE during early Oligocene metamorphism. Older Sm-Nd ages reflect mixed analyses of variably reset individual garnet crystals.

Lu-Hf isotopic analyses of bulk garnet fractions, despite yielding high parent/daughter isotopic ratios appeared very scattered and did not allow defining isochron ages. Instead, apparent ages defined by whole rock and individual garnet fractions range from c. 80 to 160 Ma. Very old apparent ages are interpreted as being the consequence of variable degree of intracrystalline Lu diffusion and preservation of the

original Hf distribution, which leads to lower $^{176}Lu/^{177}Hf$ ratios, and thus steeper (older) isochrons. Back diffusion of Lu during commonly observed resorption played subordinate role in modifying isotope systematics.

Keywords: Sm-Nd, Lu-Hf, garnet dating, trace elements, diffusion, Vietnam

1. Introduction

The application of Sm-Nd and Lu-Hf garnet geochronology offers a quantitative link between isotopic ages and metamorphic conditions. Most commonly, the link is established on the basis of major element zonation in garnet or by means of thermodynamic calculations and textural relationships (e.g. Vance and Mahar, 1998a). Such an approach is largely justified for garnets, where zonation patterns developed during growth, are preserved. In higher temperature ranges, where major element distributions can be partially or completely modified by diffusion, the interpretation of isotopic ages obtained by both geochronometers is subject to a large degree of uncertainty as a result of the likely decoupling of Rare Earth Element (REE) and High Field Strength Element (HFSE) behaviour from that of the major elements. This problem is partly overcome with *in situ* trace element analyses in garnets in high grade rocks (e.g. Anczkiewicz et al., 2007a; Dutch and Hand, 2010; Endo et al., 2009; Kohn, 2009). More recently trace element analyses of garnets have become fairly common. However, the interpretation of their record is often equivocal and relies on detailed knowledge of the textural relationship and crystallisation history of the garnet and associated minerals. Additionally, the involvement of garnet in post-growth reactions leads to the redistribution of trace elements involved in garnet

geochronology, which may lead to erroneous ages or false interpretations (e.g. Dutch and Hand, 2010; Kelly et al., 2011; Kohn, 2009). In this study we investigate the potential influence of diffusion and resorption on Sm-Nd and Lu-Hf garnet geochronology in polymetamorphic migmatitic gneisses from the Day Nui Con Voi massif in northern Vietnam.

The Sm-Nd results for V99-8 and V99-66 were previously published in Anczkiewicz and Thirlwall (2003) in the context of presenting a new leaching technique and the reader is referred there for detailed discussion of the isotope systematics of these two samples. Here, we include results from two more samples, and discuss our geochronological results from the perspective of the trace elements analyses and their geological context.

2. Regional geology

The Red River shear zone (RRSZ) is widely regarded as a major continental discontinuity dividing SE China block from the Indochina block and was interpreted either as a deeply rooted fault penetrating through the entire lithosphere (Leloup et al., 1995; Tapponnier et al., 1990) or as a fault detached at mid-crustal level (Jolivet et al., 2001). It strikes for about 1000 km from SE Tibet towards Tonkin Gulf in northern Vietnam (Fig. 1), and is defined by four, NW-SE trending, narrow, elongated high-grade metamorphic massifs, of which the Ailao Shan and the Day Nui Con Voi (DNCV) are the largest (Fig. 1).

The DNCV massif in northern Vietnam forms a large scale antiform, with strongly sheared limbs resembling a core complex type structure (Anczkiewicz et al., 2007b; Jolivet et al., 2001). It is composed dominantly of high-grade metapelitic and locally migmatitic gneisses, the peak metamorphic conditions are estimated to be 700-800 ˚C

105 at 5-9 kbars (Anczkiewicz et al., 2007b; Leloup et al., 2001; Nam et al., 1998).
106 Greenschist facies retrogression were estimated to be ~480 ˚C and ~3 kbars (Nam et
107 al., 1998).
108 Isotopic systems with high closure temperature, such as U-Th-Pb in monazite and
109 zircon, document a complex thermal history. *In situ* Th-Pb monazite dating revealed
110 strong inheritance with age components ranging from 220 to 21 Ma. The oldest age
111 was interpreted as an Indosinian event, while the younger ages were interpreted to be
112 a result of partial resetting of monazite during Oligo-Miocene (Gilley et al., 2003). In
113 the Ailao Shan massif in Yunnan, monazite included in garnets yielded ages between
114 34 and 21 Ma, interpreted as reflecting synkinematic (relatively to sinistral shear)
115 monazite and garnet growth. The older ages are the same within error as the U-Pb
116 zircon age constraints on deformed granitoids from within the southern Ailao Shan
117 massif that yielded a c. 33 Ma age. This age has also been interpreted as reflecting the
118 beginning of strike slip motion (Zhang and Schärer, 1999). Post-metamorphic cooling,
119 established predominantly by Ar-Ar and K-Ar biotite data, reveal a wide range of
120 ages but seem to indicate that the DNCV rocks cooled through c. 300 ˚C by about 23-
121 26 Ma. (Harrison et al., 1996; Leloup et al., 2001; Nam et al., 1998; Wang et al.,
122 2000). In contrast, the K-Ar and Ar-Ar hornblende and feldspar ages range from 34 to
123 27 and display quite complex age spectra (Nam et al., 1998; Wang et al., 2000). The
124 few zircon and apatite fission track ages available for the DNCV massif span ages
125 from 30 to 20 Ma and point to, at least locally, very fast cooling after high grade
126 metamorphism and sinistral shearing (Maluski et al., 2001; Viola and Anczkiewicz,
127 2008).
128

129 **3. Samples petrography and PT conditions**

Four gneisses (V99-8, V99-66, V99-67 and V02-05) were selected for petrological and geochronological studies. Their locations are marked on a simplified geological map in Fig. 2 and their GPS coordinates are given in Table 2.

Sample V99-8 comes from the Yen Binh quarry located in the vicinity of Yen Bay in the central part of the DNCV massif (Fig. 2). The quarry exposes strongly deformed high-grade gneisses forming tens of meters scale antiform with an axial planar cleavage being at places intruded by leucogranites. Gneisses are composed dominantly of quartz, biotite, plagioclase, K-feldspar and garnet. Common accessories are monazite, zircon, apatite and rarely rutile. Garnet and feldspar form porphyroclasts in a finer grained matrix of quartz and biotite (Fig. 3a). Small amounts of chlorite and muscovite formed at the expense of garnet and biotite during retrogression. Garnet usually has inclusion-rich cores comprising dominantly quartz, a substantial amount of zircon, monazite and rare biotite. Monazite is distributed throughout the entire garnet. Although, in the studied thin sections, it appeared to be more common in the marginal parts, where also silimanite inclusions are sporadically present. The remaining three samples have almost identical mineralogy but display mylonitic textures (Fig. 3 b-d).

Garnet in all samples is dominantly of almandine composition with a smaller amount of pyrope, and negligible grossular and spessartine. Electron microprobe traverses across garnet longer axes show constant compositions across nearly the entire crystal except for the edges, where a rise of almandine and spessartine is compensated by a decrease in pyrope and grossular. The Fe/(Fe+Mg) ratio follows the almandine content (Fig. 4). Flat zonation patterns throughout most of the grains indicate that the major elements were completely homogenized and the rims were equilibrated with the matrix minerals. Of all analysed garnets only one crystal from sample V99-66

revealed slightly different zonation expressed by small "bulges" of grossular in the rim area (Fig. 4b).

Geothermobarometric estimates for samples V99-8 and V02-05 and V99-66 resulted in P= 0.56 ± 0.15 GPa at T = 810 ± 60 ˚C and P = 0.70 ± 0.16 GPa at T = 820 ± 60 ˚C and T = 800±60°C at P = 7.6 ± 1.4 kbars, respectively (Anczkiewicz et al., 2007b). Similar results for the metamorphic peak were earlier obtained by (Gilley et al., 2003; Leloup et al., 2001; Nam et al., 1998), who reported slightly lower temperatures at similar pressures. Although we did not conduct *P-T* estimates for sample V99-67, the consistency of the estimated temperature range for the three other samples, their identical mineralogy and proximal location to sample V99-66, implies that this rock was metamorphosed under the same metamorphic conditions as the other analysed samples.

4. Sm-Nd and Lu-Hf garnet dating

Garnet from all four gneiss samples were dated using the Sm-Nd method and samples V99-67 and V02-05 were additionally subjected to Lu-Hf analyses. Sample dissolution, leaching procedures and column chemistry are described in Anczkiewicz and Thirlwall, (2003) and Anczkiewicz et al., (2004). All measurements were carried out using a multi-collector ICP MS IsoProbe® following procedures outlined in Thirlwall and Anczkiewicz, (2004). Isotopic results are summarised in Table 2 and Fig. 6. Analytical blank, standard reproducibility and reference isotopic ratios are given in the footnote to Table 1. Ages were calculated using Isoplot® by Ludwig, (2001). Errors for isotopic ratios are given at the 2 SE (standard error) level. Age errors, are quoted at 95% confidence level.

4.1 Sm-Nd isotopic results

A minimum of one whole rock and two garnet fractions from each sample were used for isochron constructions. Representative whole rock splits and biotite were used to determine the initial $^{143}Nd/^{144}Nd$ ratios. Samples V99-8 and V99-66 gave the same ages within error of 39.1 ± 0.8 and 41.7 ± 1.4 Ma, respectively (Anczkiewicz and Thirlwall, 2003). By contrast, sample V99-67 yielded a significantly younger age of 31.7 ± 0.9 Ma, while V02-05 gave an age of 49.8 ± 2.5 Ma.

All but one of the analysed garnet fractions yielded $^{147}Sm/^{144}Nd$ ratios between 0.97 and 2.13, which is commonly found in metamorphic garnets (e.g. Prince et al., 2000; Thöni, 2002; Vance and Harris, 1998b). Garnet Grt. 1 from V02-05 is the only one with a low $^{147}Sm/^{144}Nd$ ratio and a correspondingly low $^{143}Nd/^{144}Nd$ ratio, almost the same as the whole rock values. Fraction Grt. 1 was not treated by the sulphuric acid leaching (SAL) method and hence its Nd budget was overwhelmed by monazite inclusions, which are numerous in the studied rocks. However, even leached garnets from this sample show a significant spread among measured isotopic ratios (Table 2 and Fig. 6). This is most likely due to incomplete exposure of monazite inclusions to sulphuric acid leaching (see Anczkiewicz and Thirlwall, (2003) for discussion). Nevertheless, monazite influence must have been very small, since even the presence of as little as a few tens of ppm of this mineral in the "bulk" garnet separate would make dating impossible (e.g. Prince et al., 2000; Zhou and Hensen 1995). Grinding to smaller fractions almost certainly would significantly reduce the spread among analysed garnet separates (Anczkiewicz and Thirlwall, 2003). Some of the observed spread could also be ascribed to different proportions of garnet cores and rims in bulk separates, which have different Sm/Nd ratios (see below).

4.2 Lu-Hf isotopic results

The same garnet and whole rock fractions from samples V02-05 and V99-67, which were used for Sm-Nd analyses, were also dated by the Lu-Hf method. Garnets from both samples show high $^{176}Lu/^{177}Hf$ ratios ranging from 1.8 to 9.4, which normally ensure precise age estimates. Yet, garnet fractions from the same sample do not lie on a common isochron (Fig. 7). Ages for V02-05 based on two-point tie lines between garnet and the whole rock, are 86 and 91 Ma, whereas those for V99-67 are 142 and 164 Ma. Potential sources of scatter of apparent Lu-Hf ages and their relationship to Sm-Nd dates are discussed after introducing the results of trace element analyses.

5. Laser ablation ICP-MS results

Garnet trace-element concentrations were determined using the Open University Agilent 7500s quadrupole mass spectrometer coupled to frequency quintupled Nd:YAG UV (213 nm) laser system (UP213, Merchanteck-New Wave Research). Ablation was performed in pure He-atmosphere (0.65 ± 0.05 L/min) mixed before entering the torch with a flow of Ar (≈1.00 ± 0.05 L/min). The ICP-MS was operated with its shield torch at 1350 W and tuned to produce maximum sensitivity for the medium and high masses, while keeping the oxide production rate low ($^{248}ThO/^{232}Th \leq 1\%$). NIST glass 612 (Pearce et al., 1997) was used as the calibration standard and garnet K23 (from T. Zack) was used as a reference to monitor accuracy and inter-laboratory consistency. Microprobe CaO concentrations were used as the internal standard. Analyses were achieved using a static ablation spot size of 80 μm and a laser fluence of 3-4 J/cm^2, pulsed at a frequency of 10 Hz. Ten cycles of 10 s each were measured with gas blanks prior to each ablation spot. Each set of 8-10 unknown ablation spots was bracketed with NIST 612 glass measurements and

variations in standard intensity were interpolated between successive standard measurements.

Additional set of analyses was later performed at Institute of Geological Sciences, Polish Academy of Sciences, Kraków Research Centre with 193 nm excimer laser *Resolution M50* by Resonetics coupled with quadrupole ICP-MS *XSeriesII* by Thermo. Ablation took place in pure He (flow rate of 0.9 L/min), which was mixed with Ar nebuliser gas (flow rate of 0.5-0.55 L/min) and after passing through a signal smoothing device analyte was delivered to the ICP source. Small addition of nitrogen (0.06-0.08 L/min) was used to enhance sensitivity. Oxide level was kept below 0.5 %. Analyses were performed with spot size of 80 μm, fluence of 3-4 J/cm^2 and at repetition rate of 10 Hz. Each 40 seconds ablation time was preceded by 20 s blank and followed by 20 s washout. Sample runs were bracketed by measurements of NIST 612 glass (Pearce et al., 1997). Silica content was used as an internal standard.

Data from both laboratories were processed using Glitter software of Macquarie University, Australia (Griffin et al., 2008). Thick sections were cut parallel to the stretching lineation and perpendicular to foliation. Traverses across garnets were made along the longest axis. A summary of LA ICPMS results is presented in Fig. 8-13 and element abundances are listed in Table 2 (online supplementary material).

There are two first order features common for all analysed garnets: (1), a very clear core-to-rim zonation among HREE and, with one exception, modest zonation among LREE, (2) well pronounced negative Eu anomaly, which most likely reflects crystallization of garnet in the presence of feldspar (Fig. 8). Although chondrite

normalised plots nicely reveal primary features, many important details in distribution of REE are masked or very difficult to decipher. Hence, below we provide rim-to-rim plots with detailed descriptions of key elements from each sample. Light REE behaviour is illustrated by Nd and Sm, while heavy REE behaviour is shown with Lu. Abundance of all measured trace elements are compiled in Table 2.

5.1 Sample V99-8

Light REE rim-to-rim zonation profiles illustrated with Nd and Sm in Fig. 9a are slightly concave downwards. This is particularly well pronounced for Sm and, to a much lesser extent, for Nd (Fig. 9a). Occasionally, this trend is followed by a drop in concentration on the edges (Fig. 9a). Heavy REE (represented in Fig. 9b by Lu) show a steep decrease in concentrations from core to rim. The higher the mass of an element, the steeper the gradient (Fig. 8). While light REE on the edges show decrease of concentrations, heavy REE show rise of concentrations in the same area (Fig. 9a and b). Hafnium content smoothly increases from core to rim, while on the edges decreases similarly to LREE (Fig. 9c). Yttrium, which is commonly used as a heavy REE proxy, indeed mimics their behaviour (Fig. 9b).

5.2 Sample V99-67

Distribution of trace elements in garnets in V99-67 is similar to that described above. The main difference is confined to the LREE, which show a much smaller degree of zonation, in particular in Nd, which shows a flat rim-to-rim profile (Fig. 10a,d). Samarium shows only a slightly larger degree of zonation in larger crystals. As with sample V99-8, the largest Sm/Nd fractionation occurs on the edges due to the notable rise of Sm (Fig.10a, d). Notably, abundance of both Nd and Sm in all analysed

crystals is practically the same. Heavy REE show variable abundance and zonation trends from very steep to practically flat (Fig. 10b, e). Hafnium shows flat or gently rising concentration pattern from core to rim (Fig. 10c, f).

5.3 Sample V99-66

Three types of rim-to-rim zonation profiles were observed in this sample. The first is represented by Grt 1, in which the light REE display a steep core to rim gradient (Table 2 and Fig. 11), which is then, in some cases, followed by a decrease in concentration on the edges (Fig. 11a). Yttrium, (similarly Dy, Ho, and Er) displays low but uniform concentrations across the core and then show sharp, positive spike followed by a decrease in concentration towards the edges (Table 2 and Fig. 11b). Interestingly, Yb and Lu do not follow other heavy REE behaviour. Instead, their concentration is fairly uniform across the core and then sharply falls towards the rim, where it remains fairly constant (Fig. 11c). The presence of the distinct spikes observed for Y, Dy, Er and Ho correlates with a minimum P content (Fig. 11b). Hafnium generally increases from core to rim with an inversion of this trend on the edges. There is a small but notable elevation in Hf concentration in the centre (Fig. 11d).

The second type of zonation represented by Grt. 2 shows very similar light REE zonation patterns to Grt. 1 (Fig. 12a). The origin of some “dispersion” visible in the general trends is probably caused by the selection of ablation spots, which were forced to be shifted from the straight line in order to avoid cracks and inclusions, and thus neighbouring spots in some cases probed the same garnet zones. Heavy REE concentration steeply decreases towards the rim, which is followed by a gentle rise on

the edges (Fig. 12b). Notably, absolute concentration values for heavy REE and Y are significantly higher than those in Grt. 1. The hafnium trend is analogous with Grt. 1 described above. The only difference is that the elevation of concentration in the centre is much clearer and correlates with higher U content, which points to contamination by a U-bearing inclusion. Yttrium follows the trend of HREE (Fig. 12c). The two garnet crystals described above belong to the largest and most representative for the sample. Additionally, we analysed garnet crystals ranging from 2 to 3.5 mm. Their trace element distribution is very similar to Grt 2, although the content of both light and heavy REE is much smaller.

Rarely, crystals are observed, which are distinctly different from the ones described above. Their light REE show very little zonation, similar to garnets from V99-8 and V99-67 (Fig. 12d). By contrast, heavy REE show very different distribution patterns, having low, but fairly uniform concentrations across the crystals but with two distinct spikes in the rims (Fig. 12e). In this respect this profile resembles Y, Dy, Ho and Er in garnet Grt. 1 described above. In Grt. 3, however, the spikes are observed for all HREE and for Y. In some crystals Lu zonation is inversely correlated with P (Fig. 13). Hafnium shows rather constant concentration throughout the crystal except for the edges, where its concentration is significantly higher (Fig. 12f).

5.4 Sample V02-05

Garnets from V02-05 have dense cracks and are particularly inclusion-rich, causing some difficulties in obtaining good quality analyses. Chondrite normalized patterns display little zonation among LREE and, in contrast to garnets from other samples, modest zonation in heavy REE (Fig. 8). More detailed plots show that

elements from La to Dy have the lowest concentrations in the core, which gradually rise in the rim and then drop on the edges (e.g. Sm and Nd in Fig. 14a). Heavy REE from Ho to Lu show decreasing concentrations from core to the intermediate part of crystal and subsequently show a rise in concentrations in the rims. Yttrium broadly follows the trends of HREE. The only difference is confined to the heaviest REE, which show much clearer higher concentrations in the core (Fig. 14b). Hafnium shows a profile comparable to the LREE (Fig. 14c).

6. Discussion of LA-ICP-MS trace element analyses

Nearly all analysed garnet crystals show zonation trends suggesting Rayleigh-like fractionation mechanism, as modelled for Mn by (Hollister, 1966). It is characterized by steeply decreasing abundance of an element from core to rim forming a bell-shaped trail across a crystal. Such a profile is typical of elements, which are compatible in garnet (partition coefficient >1), while a reversed profile is expected for elements with partition coefficients <1. Modelling of Nd, Sm and Hf zonation in garnet based on Rayleigh law conducted by Kohn, (2009) suggests little zonation for incompatible elements like Nd, Sm or Hf. Indeed, studied crystals display a very smooth rise of concentration from core to rim, which becomes steeper towards the rim area. Nevertheless, the zonation trends in larger crystals are very clear, in particular for Sm, which is more compatible than Nd, and particularly Hf (Fig. 9-14). The degree of Sm and Nd zonation clearly correlates with the crystal size (Fig. 15). Rim-to-rim profiles become progressively flatter from garnets of about 7 mm size in sample V99-66, where zonation is fairly strong, to completely flat profiles in garnets of about 1 mm size in sample V99-67 (Fig. 15). On a hand specimen scale, such correlations are also present. Although the available range of garnet size is more

limited, in sample V 99-66, where size of the analysed crystals vary from about 7 to 2 mm, the light REE patterns show much stronger zonation in the larger crystals and milder among the smaller crystals. However, zonation in 2.0-3.5 mm crystals is practically the same both in terms of style as well as absolute concentrations (Fig. 16a). Smaller crystals (< 2 mm) observed in V99-67 show very little or no LREE zonation and their Nd and Sm content is the same in all analysed grains (Fig. 17a).

If garnet crystallization followed the Rayleigh distillation model, such rather regular changes of LREE zonation, on a hand specimen scale, could have been caused by progressively later nucleation of the smaller crystals as described for major elements by Kretz (1994). Indeed, with exception of sample V99-67, we find higher abundance of Sm and Nd in the cores of the smaller crystals relatively to the larger ones, which is expected for the elements preferentially partitioned into matrix (Fig. 15, 16a). This is additionally supported by the opposite trends observed for heavy REE, although the correlation is less obvious (Fig. 16b). In sample V99-67, however, we observe the same abundance and almost completely flat Nd and Sm zonation patterns throughout all studied crystals, while Lu zonation is variable, and does not seem to show any correlation with crystal size (Fig. 17). Additionally, in the case of the prolonged garnet nucleation, we would expect to see some textural variations among studied garnet. Instead, garnets regardless of their size show the same set of inclusions and the same relationship with the surrounding matrix.

Alternatively, progressive flattening of zonation profiles with the decreasing crystal size could be a result of diffusional homogenisation of Nd and Sm in garnet due to high temperature metamorphism. Such interpretation is consistent with experimental studies of Nd and Sm diffusivity, which suggest that the Sm-Nd system is, generally, open above 700 ˚C (Tirone et al., 2005) or 750 ˚C (Van Orman et al., 2002)

temperature for garnet size of 1.5 mm or smaller at moderate to fast cooling rates (noteworthy, the former study shows much stronger dependence of closure temperature on cooling rate). Similar, or even slightly lower closure temperature was estimated for HREE (Tirone et al., 2005; Van Orman et al., 2002). Preservation, of steep Lu core to rim zonation patterns even in c. 1 mm garnets, at first glance, argues against significant diffusion of this element. However, since it is not possible to verify whether the original HREE profiles were not even steeper, we cannot entirely rule out, that some intracrystalline diffusion took place. Because of much higher HREE concentrations, partial thermal relaxation of HREE is more difficult to detect. In sample V99-66, where garnet size shows the largest variations, smaller crystals have clearly flatter profiles (Fig. 16b), which suggest that intracrystalline diffusion of Lu could have taken place.

Diffusional homogenization well explains the zonation trends particularly in V99-67, where the garnets show a narrow diameter range between 1 and 2 mm. In all investigated crystals Nd and Sm lack zonation and have practically the same abundance (Fig. 17a). Lutetium, on the other hand, shows variable content and variable degree of flatness, which could also be attributed to partial thermal relaxation.

Trace element analyses alone do not allow to unequivocally decide, whether, diffusional homogenization or progressively younger garnet crystallization during Rayleigh style crystallisation is responsible for the observed trace element distribution. Combination of both cannot be ruled out either. We continue the discussion of both mechanisms in the context of the revised interpretation of the Sm-Nd and Lu-Hf dating results, below.

As already mentioned, hafnium is highly incompatible in garnet and thus, its distribution, qualitatively, is expected to be similar to light REE. Indeed, zonation of Hf in all analysed garnets shows trends analogous to those observed for Nd and Sm in larger crystals (Fig. 9-14). However, unlike the LREE, Hf zonation is still preserved even in the smallest grains, and thus most likely, was unaffected by intracrystalline diffusion, which is in accord with its very slow diffusivity (Bloch et al. 2010; Ganguly et al. 2010).

Except for diffusional homogenization and prolonged garnet nucleation that affected REE abundance and distribution, we observed other syn- and post-crystallization modifications of simple Rayleigh-like fractionation model. The most common and the most significant post growth modification, observed in all studied samples is confined to garnet rim area. It is expressed by rise in heavy and drop of light REE abundance (e.g. Grt. 1 from sample V99-8, Fig. 9). We relate this phenomenon to resorption, evidence of which is clearly visible in thin sections (Fig. 3). Redistribution of elements by resorption can be very significant. A good example is Grt. 1 from sample V02-05, where resorbed rims have heavy REE concentrations similar to these observed in the garnet centre (Fig. 14). In the case of Grt. 1 from V99-8 resorbed rims achieve concentrations more than half of those observed in the core (Fig. 14). A more typical situation in the studied samples, however, is represented by Grt. 1 from sample V99-8, where resorption could have affected about 15-20 % of the studied profile (Fig. 9). We tentatively link the resorption process to back diffusion from melt during anatectic metamorphism, which also caused intracrystalline diffusion of light REE described above. Importantly, this process creates minima near the rim in Lu zonation

429 profiles, that act as a barrier, which cannot be passed by diffusing Lu from either side.
430 Hence, Lu between the minima can be relocated but cannot escape garnet.
431
432 All other deviations from a Rayleigh-like pattern, were observed only in sample V99-
433 66 and relate to the time of garnet crystallization. In garnet Grt. 1 broad core with
434 nearly constant concentrations of Yb and Lu followed by a sudden drop of
435 concentrations resembles a profile documented by Pyle and Spear, (1999) for Y in
436 garnets from starurolite zone metapelites. The authors linked the observed pattern to
437 co-crystallization of xenotime. Adopting this type of interpretation, fairly uniform
438 abundance of Lu in the core could suggest co-crystallization of a HREE-rich mineral.
439 The third type of "anomalous" profile was observed in the same crystal and is
440 expressed by very high spikes of Y, Dy, Ho and Er, which correlate with minimum P
441 content (Fig. 11b,c). Possible interpretations of such patterns were discussed by
442 Lanzirotti (1995). Correlation of Y peaks with change in P zonation suggests that this
443 type of modification could be related to a change in a phosphate mineral being in
444 equilibrium with garnet and breakdown of a Y-rich mineral (Yang and Rivers, 2002).
445 Another important feature of this particular garnet is that the Y distribution trend is
446 not coupled with the trends of two the heaviest REE. Yttrium does not display any
447 resemblance neither with Yb nor Lu. Moreover, in the same thin section neighbouring
448 crystals show "normal" behaviour, where Y zonation is compatible with zonation of
449 all HREE. We interpret differences in zonation trends in proximate garnets as
450 resulting from small scale matrix heterogeneities and variations in reactions with
451 accessory phases.
452

453 The only analysed garnet that does not fit into any of the categories described above is
454 garnet Grt. 3 from sample V99-66. The profile is rarely found and only in the crystals
455 smaller than about 3 mm. It is practically flat with two distinct spikes near the
456 margins, similar to Y and HREE (with exception of Yb and Lu) observed in Grt. 1
457 from the same sample. Again, similarly to Grt. 1 the spikes correlate with P zonation,
458 which points to the importance of reactions involving phosphates in REE partitioning
459 and the resulting profile probably reflects small scale matrix heterogeneities.
460

461 **7. Comparison of ID and LA ICPMS results**

462 Comparison of Sm/Nd and Lu/Hf ratios obtained by isotope dilution (ID)
463 method with "true ratios" obtained by *in situ* laser ablation ICPMS allows us to
464 estimate the extent of contribution from REE- and Hf-rich inclusions to our isotopic
465 analyses. If our mineral separates were pure and sulphuric acid leaching effectively
466 removed monazite and apatite inclusions, the Sm/Nd ratios recovered by ID should be
467 close to those measured by laser ablation ICP-MS. In Fig. 18 we presented Sm/Nd
468 and Lu/Hf ratios for individual ablation spots and marked the highest ID values
469 obtained for bulk garnet separate from the same samples. The plots show excellent
470 agreement of Sm/Nd ratios measured by ID and LA ICPMS for all samples but V02-
471 05. In the latter case, *in situ* measurements show ratios twice as high as these obtained
472 by isotope dilution (Fig. 18c), which indicates that Sm-Nd dating of this sample could
473 be unreliable. Remarkable agreement in Sm/Nd ratios obtained by both techniques for
474 the remaining samples, indicates that monazite inclusions were efficiently eliminated
475 by sulphuric acid leaching during sample preparation. Some variations among
476 $^{147}Sm/^{144}Nd$ ratios in different garnet fractions are interpreted as resulting primarily
477 from different proportions of core and rim in bulk separate, but also from certain,

rather minor, contribution from inclusions (e.g. feldspar or biotite), which is unavoidable.

At first glance it may seem that Lu/Hf ratios obtained by ID analyses, do not reproduce "true" Lu/Hf ratios determined by LA ICPMS (Fig. 18). However, the departure from "true value" is subjected to large uncertainty due to very strong Lu zonation. Except for comparing Lu/Hf ratios, the influence of Hf-rich inclusions can additionally be controlled by comparison of Hf concentrations derived by LA ICPMS and ID methods. In the case of sample V99-67, the ID method recorded 200 and 300 ppb Hf concentration in comparison to about 100 ppb obtained by laser ablation (Table 1 and Fig. 10). Thus, some influence of inherited Hf could explain lower Lu/Hf ratios recorded by isotope dilution in garnets and additionally contributed to strong scatter observed in the isochron diagram (Fig. 7). In the case of sample V02-05, however, both techniques point to about 100 ppb Hf concentration, which indicates, that Lu/Hf ratios in this sample measured by ID reflect rather clean garnet separates (Table 1 and Fig. 14) and points to some other source of scatter among the Lu-Hf analyses. We develop this topic in the next section.

8. Interpretation of garnet dating results in the context of trace element analyses

Combining Lu-Hf and Sm-Nd isotopic analyses with *in situ* laser ablation ICPMS measurements of trace elements abundance, puts a new perspective on the interpretation of Lu-Hf and Sm-Nd garnet dating from the DNC gneisses. Geochronology, on the other hand, helps to understand some of the REE zonation features in garnet (see below). In the case of Sm-Nd dating LA ICP-MS document two key features. Firstly, remarkable agreement of Sm/Nd ratios measured by LA ICPMS and isotope dilution shows that garnet separates were very well purified prior

503 to analyses and mixing with any inherited Nd cannot be a reason for the observed
504 large age variations. Secondly, progressive flattening of the Nd and Sm zonation
505 profiles with decreasing garnet size indicates that diffusional homogenization, and
506 thus variable (size dependent) degree of resetting in garnets, is the most likely cause
507 of the observed age differences (Fig. 15). Some contribution to the observed pattern
508 could be caused by prolonged growth of progressively smaller garnets (Kretz, 1994).
509 In samples V99-8 and V99-66 garnet size varies from about 2 mm to more than
510 couple of cm (with a median size of about 3 and 5 mm, respectively). Hence, despite
511 the fact that isochrons defining both ages are of very good quality, they are unlikely to
512 date any specific geological episode (regardless of the reason for the variation in Nd
513 and Sm distribution). In both cases they represent a mixture of variably reset
514 individual garnet crystals (or a mixture of grains nucleating over a prolonged time
515 period) and provide a minimum age for early garnet growth and a maximum age for a
516 resetting episode (or the youngest growth).

517 The time of the resetting episode is best approximated by the youngest 31.7±0.9
518 Ma age recorded by V99-67. In the latter sample the largest crystals are about 2 mm,
519 while the majority are smaller than 1.5 mm. All analysed garnets practically lack
520 zonation and show the same Nd and Sm abundance, which we interpret as a result of
521 diffusional homogenization (Fig. 17a).

522 A similar phenomenon has been recently reported by Dutch and Hand (2010) who
523 observed younging of garnet ages with decreasing crystal size in an early Proterozoic
524 granite due to a high temperature overprint. The authors explained the observed
525 pattern by higher closure temperatures in larger crystals. At the same time, they note
526 that REE were not mobilised, which may indicate that some mechanism other than
527 diffusion could be responsible for larger degrees of resetting in smaller crystals.

528 The question arises, how accurately the youngest sample dates the resetting
529 episode. The cooling rates for early evolution of DNCV based on available
530 thermochronology vary from about 100 °C/Ma (Nam et al. 1998) to about 50 °C/Ma
531 (Leloup et al. 2001). Using computer program of Ganguly and Tirone (1999) and
532 thermodynamic data of Tirone et al. (2005), we estimated closure temperature T_c for
533 Nd in 1 mm diameter garnet undergoing cooling from peak temperature T_o = 800 °C
534 at rates between 50 and 100 °C/Ma as 713-724 °C (Fig. 19). Analogous estimates for
535 garnets of 7 mm diameter results in T_c just 10-15 °C below the temperature peak.
536 Thus, because closure temperature in V99-67 garnets is significantly below the
537 temperature peak, the estimated age should reflect early cooling phase. Accepting
538 cooling rates mentioned above, about 2.1 to 4.6 Ma of age resetting during cooling
539 could have taken place (calculated using computer program of Ganguly and Tirone,
540 1999, and thermodynamic data of Tirone et al., 2005). As mentioned above, cooling
541 rate is a subject of some speculation but it is likely to be on the higher side of the
542 proposed range. This is suggested by the oldest zircon and apatite fission track ages,
543 which range from 30 to 25 Ma (Viola and Anczkiewicz 2008) and are only slightly
544 younger than Sm-Nd garnet age presented here. Thus, the temperature peak, occurred,
545 probably, some 2 Ma earlier than Sm-Nd closure in V99-67 garnets.
546
547 Lu-Hf dating did not provide isochron ages. High scatter of the analyses in both
548 samples does not permit defining an age for any of them. An obvious possibility of
549 data scatter that has to be considered is contamination by inherited Hf from zircon
550 inclusions, which are numerous in garnets and in the matrix. Mixing of inherited Hf
551 from zircons with Hf from garnets tends to lower the measured $^{176}Hf/^{177}Hf$ and
552 $^{176}Lu/^{177}Hf$ ratios, reducing the slope of an isochron and resulting in artificially

553 younger ages (e.g. Prince et al., 2000; Scherer et al., 2000). This view is correct
554 providing initial $^{176}Hf/^{177}Hf$ was determined accurately. However, whole rock splits
555 used for estimating initial $^{176}Hf/^{177}Hf$ ratio are affected by inherited zircons too.
556 Hence, "too low" $^{176}Hf/^{177}Hf$ ratios in the whole rocks, could make isochrons steeper
557 and thus, artificially, "too old" (providing garnet ratios were accurate). A hint of
558 which of the two scenarios prevailed is provided by $\varepsilon Hf_{CHUR}(t)$ for tie lines defined
559 separately by each garnet fraction with the whole rock. They give values of -8 and -10
560 for sample V99-67, and -11 and -12 for sample V02-05 (calculated using reference
561 ratios of Bouvier et al., 2008). Such values are expected for metasedimentary rocks
562 and correlate well with the corresponding $\varepsilon Nd_{CHUR}(t)$ of -13.0 and -10.9 for the same
563 samples (calculated using reference values of Jacobsen et al., 1980). Hence, we can
564 assume that initial ratios, although certainly, to some extent, influenced by Hf
565 scavenged from zircons (digestion took place on a hotplate, which limits zircon
566 dissolution), are reasonably well constrained and thus, the major source of potential
567 age inaccuracy we ascribe to Lu-Hf analyses of garnet fractions. It is also noteworthy,
568 that in the case of high parent/daugther ratios in garnet, accuracy of initial ratio
569 determination for the Lu-Hf decay system is a lot less critical than for Sm-Nd because
570 of significantly higher ratios of the former system. Isotopic ratios in garnet fractions
571 show spread large enough, to provide age estimates based on garnets alone. They
572 define 84.1±2.3 Ma age for sample V99-67 and 77.0±1.9 Ma for sample V02-05 (Fig.
573 7). Although dates are somewhat similar, their hugely positive $\varepsilon Hf_{CHUR}(t)$ of about
574 105 and 50 are unrealistic, and thus both two garnets tie lines ages are undoubtedly
575 false.
576

577 Although, at least in the case of sample V02-05 we cannot rule out some inherited Hf
578 mixing, we do not consider this as a main reason for the observed complexities of our
579 Lu-Hf dating efforts. Applying the same way of reasoning as with Sm-Nd system,
580 extended in time garnet nucleation should be taken into account as a mechanism
581 responsible for the observed systematics. Individual apparent garnet ages, would
582 represent a mixture of crystals defining the minimum age for the beginning of
583 crystallization. However, if protracted garnet crystallization was the only operative
584 mechanism, we would expect to observe good degree of similarity of the Lu-Hf and
585 the Sm-Nd ages obtained for the same fractions. These, however, show dates up to
586 about 100 Ma younger. Thus, prolonged garnet crystallisation of progressively
587 smaller crystals alone does not explain the observed REE zonation patterns and the
588 obtained ages.
589 Under high temperature conditions much faster diffusion of Lu relative to Hf
590 combined with garnet dissolution could lead to lower $^{176}Lu/^{177}Hf$ ratios, while keeping
591 the same $^{176}Hf/^{177}Hf$ ratios, causing "counter clockwise rotation" of isochrons, thus
592 increasing the apparent Lu-Hf ages (Kohn, 2009; Ganguly et al. 2010). Because this
593 process also depends on crystal size, variable degrees of resetting could potentially
594 lead to the observed scatter and shift Lu-Hf ages towards older ranges. Such an
595 interpretation is particularly appealing, especially, when taking into account the high
596 temperature of metamorphism, much younger Sm-Nd ages and almost the same
597 diffusivity of light and heavy REE postulated by the experimental data (Tirone et al.,
598 2005; Van Orman et al., 2002). Our LA ICP-MS data seem to support such scenario.
599 Although Lu still shows very clear zonation in most of the small crystals, this could
600 be due to the fact that their original pattern was considerably stronger than that of
601 LREE and complete homogenisation did not take place. Hafnium on the other hand,

602 rather consistently shows one type of profile and likely preserved disequilibrium
603 growth conditions (with some minor modifications particularly in the rim area, see
604 above). Thus, thermally driven intracrystalline diffusion of Lu combined with very
605 "stationary" Hf behaviour, could lead to the counterclockwise rotation of the isochron
606 and to the observed much older apparent Lu-Hf ages (Kohn 2009, Ganguly et al.
607 2010). Additional factor that has to be taken int account is resorption. Back diffusion
608 of Lu into garnet and loss of Hf during high temperature dissolution, makes Lu/Hf
609 ratios higher and leads to "younging" of original crystallization ages (Kelly et al.,
610 2011). Bearing in mind that we conducted Lu-Hf analyses of only two samples, we
611 note that garnet separates from sample V02-05, which underwent a significantly
612 larger degree of resorption (see trace element zonation in Fig. 10 and Fig. 14), does
613 show much younger ages, as expected in the sample with larger degree of resetting.
614 Thus, we observe two counteracting processes (intracrystalline diffusion and
615 resorption), which did not allow to obtain meaningful Lu-Hf isochron dates.

616 Habler et al. (2007) and Bestmann et al. (2008) showed that development of
617 micro-scale deformation zones in garnet may be a significant factor affecting garnet
618 dating results. Our study of deformation fabrics was limited to optical microscopy and
619 BSE imaging, and does not allow us to decide, whether deformation could have
620 significantly contribute to the observed microgeochemistry and isotope systematics.
621 Application of more advanced techniques would certainly help, but this was beyond
622 the scope of this study.

623

624 **9. Implications for timing of metamorphism in the Red River shear zone**

625 Timing of metamorphism and shearing in the Red River shear zone was
626 previously constrained mainly by indirect estimates using U-Pb zircon dating of

granitic melts from the Ailao Shan massif in China (Schärer et al., 1990; Schärer et al., 1994; Zhang and Schärer, 1999). Schärer et al., (1990) and Schärer et al., (1994) reported ages between 26 and 22 Ma for vast majority of dated granitic dykes. One of these dykes, outside the main shear zone but following its trend, was dated at 35 Ma and interpreted as a minimum age for the onset of left lateral shearing, which continued until 20 Ma. Similar time constraints were estimated by (Zhang and Schärer, 1999) who reported ages between 33 and 22 Ma applying the same technique and similarly interpreted this time interval as the duration of left lateral shear along the RRF. *In situ* Th-Pb dating of monazite included in garnets from northern segments of RRSZ in Yunnan province in China gave very similar result to the U-Pb dating ranging from 34 to 21 Ma (Gilley et al., 2003). On the basis of microstructural and petrological observations, the latter authors linked dated monazites to synkinematic garnet growth, which led them to the conclusion that left lateral shearing started at 34 and continued until 21 Ma. The same approach applied to DNCV massif defining the southern segment of the fault, appeared inconclusive. Th-Pb monazite ages showed scatter from >200 to 20 Ma, which revealed severe inheritance problems. Large variations among monazite ages included in garnets, were interpreted by Gilley et al., (2003) as suggesting multiple garnet growth episodes. Anczkiewicz et al., (2007b) obtained 40 Ma Sm-Nd garnet ages and interpreted them as a record of an early extensional event contemporaneous with emplacement of highly potassic intrusions in SE Asia also dated at 40-30 Ma (Chung et al., 1997 and references therein). Additional garnet dating along with trace element analyses presented in this contribution places a different perspective on the interpretation of garnet ages. Thanks to trace element analyses, we could demonstrate that age variations result from thermal relaxation and possibly also from prolonged garnet nucleation under high

652 temperature conditions. In the case of Lu only partial diffusional homogenization took
653 place, while Nd and Sm in sample V99-67 underwent complete or nearly complete
654 relaxation as indicated by the same abundance and homogenous distribution of both
655 elements in all garnet crystals. Consequently, only garnets of the smallest size provide
656 best time information on the resetting event. The obtained 31.7±0.9 Ma age is about 2
657 Ma younger than the postulated age of Oligocene metamorphism in the Ailao Shan
658 massif (Gilley et al., 2003). However, when taking into account about 2 to 5 Ma age
659 resetting during cooling (see above), we can postulate, that metamorphic peak and left
660 lateral shearing in both DNCV and the Ailao Shan occurred approximately at the
661 same time.
662
663 **10. Conclusions**
664 Migmatitic gneisses in the Day Nui Con Voi massif bear a record of
665 polymetamorphic history of Indochina. Geothermobarometric calculations determined
666 conditions of the last high-grade metamorphism as 760-810 °C at 6-10 kbars pressure.
667 High temperature conditions lead to complex Lu-Hf and Sm-Nd isotope systematics,
668 which are better understood in the context of in situ trace element distribution
669 analyses in garnet. While major elements record diffusive profiles, REE and Hf
670 display a Rayleigh-like fractionation style with significant impact of post-garnet
671 crystallization modifications. Rim-to-rim zonation profiles of Nd and Sm show
672 progressive flattening with the decreasing crystal size, being completely homogenized
673 in garnets smaller than about 1.5 mm. Similar correlation, although not so well
674 pronounced, was documented for HREE. The observed correlation is interpreted as a
675 combination of relatively long lasting crystallization of progressively smaller garnets
676 and intracrystalline diffusion. Complete diffusional homogenization of Lu did not

677 occur due to much higher initial abundance and concentration gradient of this
678 element, because of its high compatibility in garnet. Both Nd and Sm show identical
679 behaviour, which is in accord with the experimental data postulating the same
680 diffusivity of these elements. Thus, 31.7±0.9 Ma Sm-Nd garnet age obtained for the
681 sample with the smallest crystal size, where light REE show flat profiles, is
682 interpreted as providing best time estimate for high temperature resetting episode
683 related to the Early Oligocene metamorphism in the Red River shear zone. The
684 obtained date is in excellent agreement with the proposed timing of metamorphism
685 and the beginning of left lateral shearing in the Ailao Shan massif, northern
686 continuation of the Red River shear zone. Older Sm-Nd ages are interpreted as mixed
687 analyses of variably reset individual garnet crystals.
688
689 Lu-Hf isotopic analyses, despite yielding high parent/daughter isotopic ratios
690 appeared very scattered and did not define isochrons. Ages derived for individual
691 garnet fractions range from about 80 to 160 Ma and are interpreted as being a
692 consequence of very different diffusive properties of Lu and Hf (Ganguly et al.,
693 2010). Intracrystalline diffusion of Lu combined with practically immobile Hf, leads
694 to counterclockwise rotation and older apparent ages (Kohn 2009). A commonly
695 observed resorption, on the other hand, tends to make ages younger (Kelly et al.,
696 2011). However, backdiffusion of Lu during resorption typically shows relatively
697 small enrichment and is typically limited to a very narrow rim area, which makes its
698 influence on isotope systmatics relatively small. These two counteracting processes
699 did not permit to obtain meaningful Lu-Hf dates.
700

Thus, only the youngest Sm-Nd age obtained for the smallest crystals, where Nd and Sm show practically complete thermal relaxation, are interpret as geologically meaningful. Taking into account that closure temperature for the Sm-Nd system in 1 mm garnet was estimated to be some 80 °C below the temperature peak, the 31.7±0.9 Ma age is interpreted as cooling from Oligocene high grade metamorphism in the DNCV massif. Taking into account some 2 to 5 Ma of cooling related age resetting, metamorphism in the DNCV and the Ailao Shan massifs, that delineate most of the Red River shear zone, occurred approximately at the same time.

Acknowledgements

R. Anczkiewicz acknowledges funding by Polish Research Grant Committee, project no. 6PO4D 011 18. Discussions with Summit Chakraborty as well as the reviews by Jibamitra Ganguly and an anonymous reviewer helped to improve the manuscript.

References:

Anczkiewicz, R., Mazur, S., Szczepanski, J., Storey, C., Crowley, Q., Villa, I.M. and Thirlwall, M.F., 2007a. Lu-Hf geochronology and trace element distribution in garnet: Implications for uplift and exhumation of ultra-high pressure granulites in the Sudetes, SW Poland. Lithos, 95 (3-4): 363-380.

Anczkiewicz, R., Platt, J.P., Thirlwall, M.F. and Wakabayashi, J., 2004. Franciscan subduction off to a slow start: Evidence from high-precision Lu-Hf garnet ages on high-grade blocks. Earth and Planetary Science Letters, 225 (1-2): 147-161.

725 Anczkiewicz, R. and Thirlwall, M.F., 2003. Improving precision of Sm-Nd garnet
726 dating by H_2SO_4 leaching- a simple solution to phosphate inclusions problem.
727 In: D. Vance, W. Mueller and I.M. Villa (Editors), Geochronology: Linking
728 the Isotopic Record with Petrology and Textures. Journal of Geological
729 Society, London, Special Publications., pp. 83-91.
730 Anczkiewicz, R., Viola, G., Muentener, O., Thirlwall, M.F., Villa, I.M. and Quong,
731 N., 2007b. Structure and shearing conditions in the Day Nui Con Voi massif:
732 Implications for the evoution of the Red River shear zone in northern Vietnam.
733 Tectonics, 26: TC2002 doi: 10.1029/2006TC001972.
734 Bestmann, M., Habler, G., Heidelbach, F., Thöni, M., 2008. Dynamic recrystallization
735 of garnet and related diffusion process. Journal of Structural Geology, 30: 777-
736 790.
737 Bloch, E., Ganguly, J., Hervig, R., 2010, Diffusion kinetics of Hafnium in garnet:
738 Experimental determination and geochronological implications. Goldschmidt
739 Conference Abstracts, A97.
740 Bouvier, A., Vervoort, J.D. and Patchett, P.J., 2008. The Lu-Hf and Sm-Nd isotopic
741 composition of CHUR: constraints from unequilibrated chondrites and
742 implications for the bulk composition of terrestrial planets. Earth and
743 Planetary Science Letters, 273((1-2)): 48-57.
744 Chung, S.L., Lee, T.Y., Lo, C.H., Wang, P.I., Chen, C.Y., Nguyen, T.Y., Tran, T.H.
745 and Wu, G., 1997. Intraplate extension prior to continental extrusion along the
746 Ailao Shan-Red River shear zone. Geology, 25: 311-314.
747 Dutch, R. and Hand, M., 2010. Retention of Sm-Nd isotopic ages in garnets subjected
748 to high-grade thermal reworking: implications for diffusion rates of major and

749 rare earth elements and the Sm-Nd closure temperature in garnet.
750 Contributions to Mineralogy and Petrology, 159: 93-112.
751 Endo, S., Wallis, S., Hirata, T., Anczkiewicz, R., Platt, J.P., Thirlwall, M.F. and
752 Asahara, Y., 2009. Age and early metamorphic history of the Sanbagawa belt:
753 Lu-Hf and P-T constraints from the Western Iratsu eclogite. Journal of
754 metamorphic geology, 27(5): 371-384.
755 Ganguly, J., Tirone, M. and Hervig, R.L., 1998. Diffusion kinetics of samarium and
756 neodymium in garnet, and a method for determining cooling rates of rocks.
757 Science, 281: 805-807.
758 Ganguly, J., Bloch E., Ito, M., 2010. Experimental diffusion kinetics of
759 geochronological systems and interpretations of mineral ages in terrestrial
760 rocks and meteorites. GSA Denver Annual Meeting, Paper no. 135-2.
761 General Geological Department of the Democratic Republic of Vietnam1973.
762 Geological Map of Vietnam (the northern part), scale 1: 1,000,000, Hanoi.
763 Gilley, L.D., Harrison, T.M., Leloup, P.H., Ryerson, O.M., Lovera, O.M. and Wang,
764 J., 2003. Direct dating of left-lateral deformation along the Red River shear
765 zone, China and Vietnam. Journal of Geophysical Research, 108(B2): 20127,
766 doi: 10.1029/2001JB001726.
767 Habler, G., Thöni, M., Muller, C., 2007. Major and trace element chemistry and Sm-
768 Nd age correlation of magmatic pegmatite garnet overprinted by eclogite
769 facies metamorphism. Chemical Geology, 241: 4-22.
770 Harrison, T.M., Leloup, P.H., Ryerson, O.M., Tapponnier, P. and Wenji, C., 1996.
771 Diachronous initiation of transtension along the Ailao Shan-Red River shar
772 zone, Yunnan and Vietnam. In: A. Yin and T.M. Harrison (Editors), The
773 tectonic evolution of Asia. Cambridge University Press, pp. 208-225.

774 Hollister, L.S., 1966. Garnet zoning: an interpretation based on Rayleigh fractionation
775 model. Science, 154: 1647-1651.
776 Jolivet, L.O., Beyssac, O., Goffe, B., Avigad, D., Lepvrier, C., Maluski, H. and
777 Thang, T.T., 2001. Oligo-Miocene midcrustal subhorizontal shear zone in
778 Indochina. Tectonics, 20: 46-57.
779 Kelly, E.D., Carlson, W.D. and Connelly, J.N., 2011. Implications of garnet
780 resorption for the Lu-Hf geochronometer: An example from the contact
781 aureole of the Makhavinekh Lake Pluton, Labrador. Journal of Metamorphic
782 Geology (in press).
783 Kohn, M., 2009. Models of garnet differential geochronology. Geochimica et
784 Cosmochimica Acta, 73: 170-182.
785 Kretz, R., 1994. Metamorphic crystallization. John Willey & Sons, 507 pp.
786 Leloup, P.H., Arnaud, N., Lacassin, R., Kienast, J.R., Harrison, T.M., Pan Trong,
787 T.T., Replumaz, A. and Tapponnier, P., 2001. New constraints on the
788 structure, thermochronology, and timing of the Ailao Shan-Red River shear
789 zone, SE Asia. Journal of Geophysical Research, B, Solid Earth and Planets,
790 106(4): 6683-6732.
791 Leloup, P.H., Lacassin, R., Tapponnier, P., Schärer, U., Dalai, Z., Xiaohan, Z.,
792 Liangshang, Z., Shaocheng, J. and Trinh, P.T., 1995. The Ailao Shan-Red
793 River shear zone (Yunnan, China), Tertiary transform boundary of Indochina.
794 Tectonophysics, 251: 3-84.
795 Ludwig, K.R., 2001. Isoplot/Ex: A Geochronological Toolkit for Microsoft Excel.
796 Special publication no. 1a, Berkeley Geochronological Centre, Berkeley, C.A.
797 Maluski, H., Lepvrier, C., Jolivet, L., Carter, A., Roques, D., Beyssac, O., Tang, T.T.,
798 Thang, N.D. and Avigad, D., 2001. Ar-Ar and fission track ages in the Song

799 Chay Massif: Early Triassic and Cenozoic tectonics in northern Vietnam.
800 Journal of Asian Earth Sciences, 19: 233-248.
801 Nam, T.N., Toriumi, M. and Itaya, T., 1998. P-T-t paths and post-metamorphic
802 exhumation of the Day Nui Con Voi shear zone in Vietnam. Tectonophysics,
803 290: 299-318.
804 Prince, C.I., Kosler, J., Vance, D. and Günther, D., 2000. Comparison of laser
805 ablation ICP-MS and isotope dilution REE analyses - implications for Sm-Nd
806 garnet geochronology. Chemical Geology, 168: 255-274.
807 Pyle, J.M. and Spear, F.S., 1999. Yttrium zoning in garnet: Coupling of major and
808 accessory phase during metamorphic reactions. Geological Research
809 Materials, 1: 1-49.
810 Schärer, U., Tapponnier, P., Lacassin, R., Leloup, P.H., Zhong, D. and Ji, S., 1990.
811 Intraplate tectonics in Asia; a precise age for large-scale Miocene movement
812 along the Ailao Shan-Red River shear zone, China. Earth and Planetary
813 Science Letters, 97(1-2): 65-77.
814 Schärer, U., Zhang, L. and Tapponnier, P., 1994. Duration of strike-slip movements in
815 large shear zones: The Red River belt, China. Earth and Planetary Science
816 Letters, 126: 379-397.
817 Scherer, E.E., Cameron, K.L. and Blichert-Toft, J., 2000. Lu-Hf garnet
818 geochronology: Closure temperature relative to the Sm-Nd system and the
819 effects of trace mineral inclusions. Geochimica et Cosmochimica Acta,
820 64(19): 3413-3432.
821 Tapponnier, P., Lacassin, R., Leloup, P.H., Schärer, U., Zhong, D., Wu, H., Liu, X.,
822 Ji, S., Zhang, L. and Zhong, J., 1990. The Ailao Shan/Red River metamorphic

belt; Tertiary left-lateral shear between Indochina and South China. Nature (London), 343(6257): 431-437.

Thirlwall, M.F. and Anczkiewicz, R., 2004. Multidynamic isotope ratio analysis using MC-ICP-MS and the causes of secular drift in Hf, Nd and Pb isotope ratios. International Journal of Mass Spectrometry, 235(1): 59-81.

Thöni, M., 2002. Sm-Nd isotope systematics in garnet from different lithologies (Eastern Alps): age results, and an evaluation of potential problems for garnet Sm-Nd chronometry. Chemical Geology, 185: 255-281.

Tirone, M., Ganguly, J., Dohmen, R., Langenhorst, F., Hervig, R. and Becker, H.-W., 2005. Rare-earth diffusion kinetics in garnet: experimental studies and applications. Geochimica et Cosmochimica Acta, 69: 2385-2398.

Van Orman, J.A., Grove, T.L., Shimizu, N. and Layne, G.D., 2002. Rare earth element diffusion in a natural pyrope single crystal at 2.8 GPa. Contributions to Mineralogy and Petrology, 142: 416-424.

Vance, D. and Harris, N., 1998b. Timing of prograde metamorphism in the Zanskar Himalaya. Geology, 27: 395-398.

Vance, D. and Mahar, E., 1998a. Pressure-temperature paths from P-T pseudosections and zoned garnets: potential, limitations and examples from the Zanskar Himalaya, NW India. Contributions to Mineralogy and Petrology, 132: 225-245.

Viola, G. and Anczkiewicz, R., 2008. Exhumation history of the Red River shear zone in northern Vietnam: New insights from zircon and apatite fission track analysis. Journal of Asian Earth Sciences, 33: 78-90.

Wang, P.L., Lo, C.H., Chung, S.L., Lee, T.Y., Lan, C.Y. and Thang, T.V., 2000. Onset timing of left-lateral movement along the Ailao Shan-Red River Shear

Zone: 39Ar-40Ar dating constraint from the Nam Dinh Area, northeastern Vietnam. Journal of Asian Earth Sciences, 18: 281-292.

Yang, P. and Rivers, T., 2002. The origin of Mn and Y annuli in garnet and the thermal dependence of P in garnet and Y in apatite in calc-pelite and pelite, Gagnon terrane, western Labrador. Geological Research Materials, 4(1): 1-35.

Zhang, L. and Schärer, U., 1999. Age and origin of magmatism along the Cenozoic Red River shear belt, China. Contributions to Mineralogy and Petrology, 134: 67-85.

Zhou, B. and Hensen, B.J., 1995. Inherited Sm/Nd isotope components preserved in monazite inclusions within garnets in leucogneisses from East Antarctica and implications for closure temperature studies. Chemical Geology, 121(317-326).

Figure captions

Fig. 1. Tectonic sketch of SE Asia (based on Leloup et al., 1995). RRF- Red River Fault. Main metamorphic massifs in the Red River shear zone: X.L.S- Xuelong Shan, D.C.S- Diancang Shan, D.N.C.V- Day Nui Con Voi.

Fig. 2. Simplified geological map of the Red River shear zone in Northern Vietnam (based on (General Geological Department of the Democratic Republic of Vietnam1973)).

Fig. 3. Photomicrographs of the analysed samples a) V99-8, b) V99-66, c) V99-67, d) V02-05. Abbreviations: Grt.- garnet, Biot- biotite, Fs- feldspar, q- quartz, Sill- sillimanite.

Fig. 4. Major element zonation profiles in garnets from sample V99-66. Garnet A represents typical zonation pattern recorded in all remaining samples. Garnet B differs

873 from other analysed crystals by the presence of small calcium “buldges” in the rim
874 area (see text for details).
875
876 Fig. 6. Sm-Nd isochron diagrams.
877 Fig. 7. Lu-Hf isochron diagrams.
878 Fig. 8. Representative rim-to-rim chondrite normalised Rare Earth Elements plots of
879 garnets.
880 Fig. 9. Rim-to-rim zonation profiles of trace elements in garnets from sample V99-8.
881 Fig. 10. Rim-to-rim zonation profiles of two garnet crystsls from sample V99-67: Sm
882 and Nd (a, d), Y and Lu (b, e) and Hf (c, f).
883 Fig. 11. Rim-to-rim zonation profiles in garnet Grt. 1 from sample V99-66.
884 Fig. 12. Rim-to-rim trace element zonation profiles of Grt. 2 (a-c) and Grt. 3 (d-f)
885 from sample V99-66.
886 Fig. 13. Rim-to-rim trace element zonation profiles of Grt. ? from sample V99-66.
887 Note inverse correlation of Lu and P.
888 Fig. 14. Rim-to-rim trace element zonation profiles in garnet from sample V02-05.
889 Fig. 15. Nd and Sm rim-to-rim zonation profiles of garnets in dependence on their
890 size.
891 Fig. 16. Sm and Lu rim-to-rim zonation profiles of garnets in dependence on their size
892 from V99-66.
893 Fig. 17. Nd, Sm and Lu rim-to-rim zonation profiles of garnets in dependence on their
894 size from V99-67.
895 Fig. 18. Rim-to-rim Sm/Nd and Lu/Hf ratios zonation in garnets measured by LA
896 ICPMS .

897 Fig. 19. Nd closure temperature Tc profiles for 1mm diameter garnet for 50 and 100
898 °C/Ma cooling rates. Dashed lines indicate mean closure temperatures. See text for
899 details.
900
901 Table 1. Sm-Nd and Lu-Hf dating results.
902 Footnote to Table 1:
903 Errors on isotopic ratios are 2SE and refer to the last significant digits. Errors for
904 $^{147}Sm/^{144}Nd$ and $^{176}Lu/^{177}Hf$ ratios are 0.3 and 0.5%, respectively. Mass bias
905 correction to $^{179}Hf/^{177}Hf$= 0.7325 and $^{146}Nd/^{144}Nd$=0.7219. Repeated measurements of
906 JMC475 standard $^{176}Hf/^{177}Hf$, over the period of analyses were $^{176}Hf/^{177}Hf$=
907 0.282176±31 (2 s.d., error, n=20) and were normalized to value $^{176}Hf/^{177}Hf$
908 =0.282160. Reproducibility of Aldrich Nd standard over period of analyses was
909 $^{143}Nd/^{144}Nd$= 0.511364±34 (2 s.d., n= 23) and were normalized to preferred value of
910 $^{143}Nd/^{144}Nd$= 0.511420. Details on long term instrument performance can be found in
911 (Thirlwall and Anczkiewicz, 2004).
912
913 Table 2. Laser ablation rim-to-rim trace element zonation profiles in garnets.

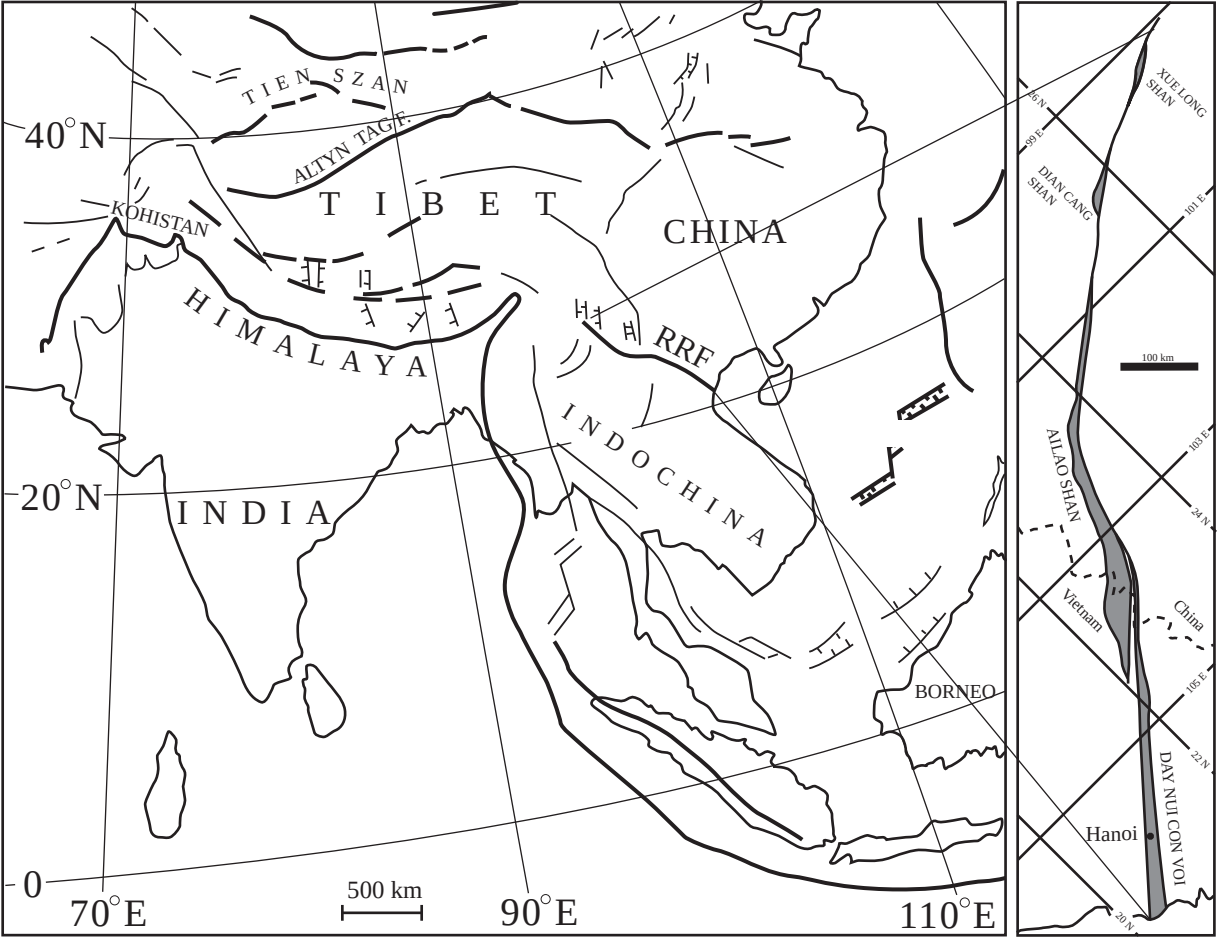

Fig. 1. Tectonic sketch of SE Asia (based on Leloup et al. 1995). RRF- Red River Fault. Main metamorphic massifs in the Red River shear zone: X.L.S- Xuelong Shan, D.C.S- Diancang Shan, D.N.C.V- Day Nui Con Voi.

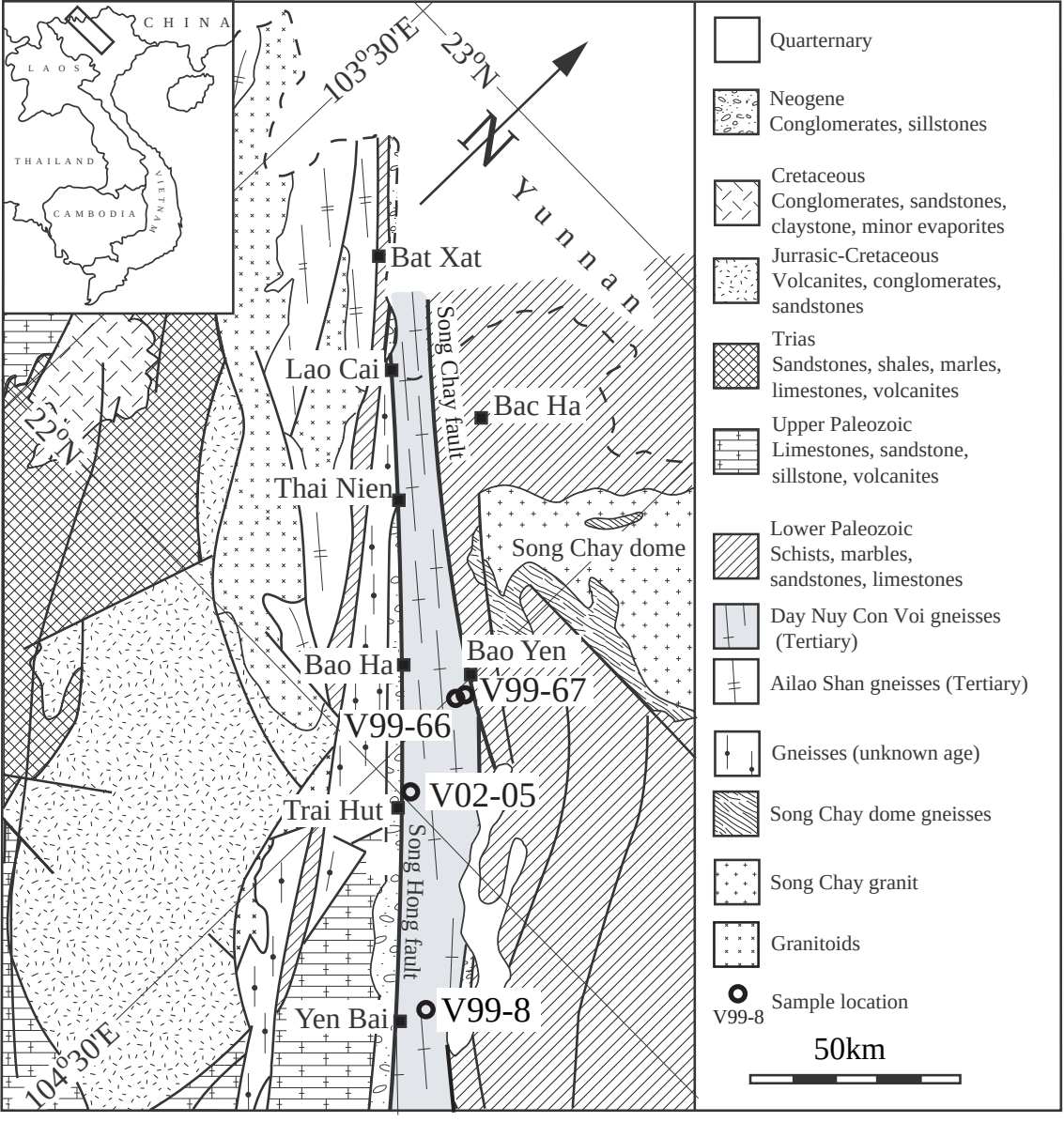

Fig. 2. Simplified geological map of the Red River shear zone in Northern Vietnam (based on the 1: 1.000.000 geological map of Vietnam, Geological Survey of Vietnam).

Fig. Anczkiewicz et al.

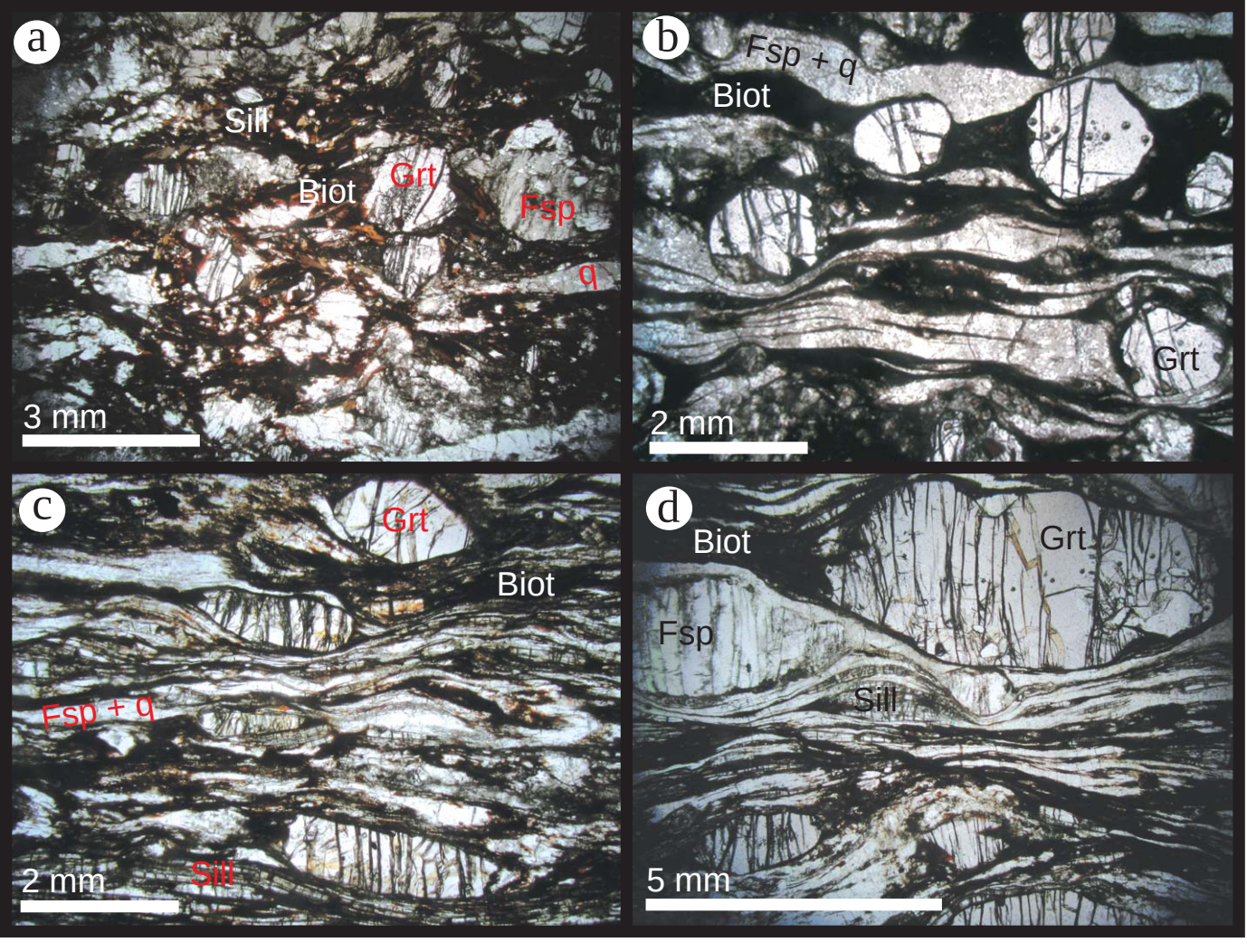

Fig. 3. Photomicrographs of the analysed samples a) V99-8, b) V99-66, c) V99-67, d) V02-05.

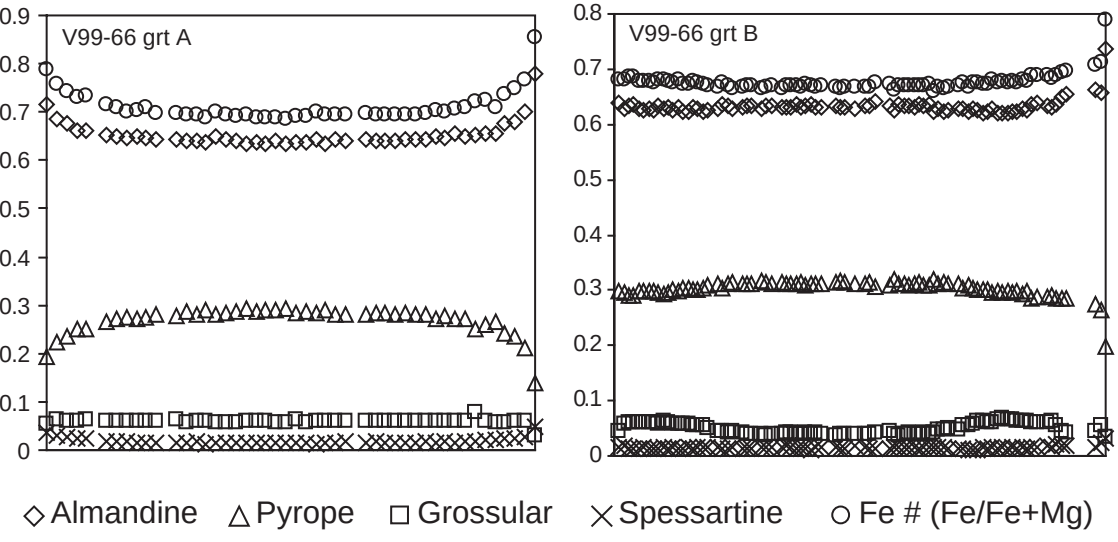

Fig. 4. Major element zonation profiles in garnets from sample V99-66. Garnet A represents typical zonation pattern recorded in all remaining samples. Garnet B differs from other analysed crystals by the presence of small Calcium “buldges” in the rim area (see text for details).

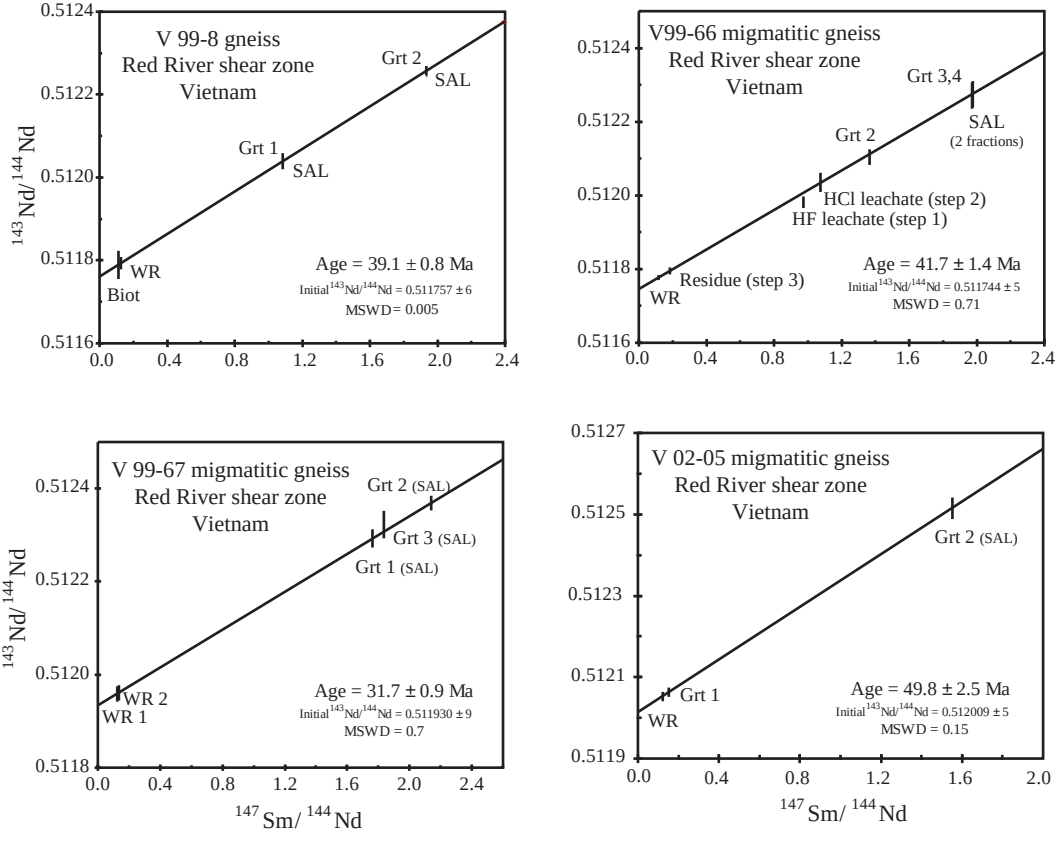

Fig. 6. Sm-Nd isochron diagrams.

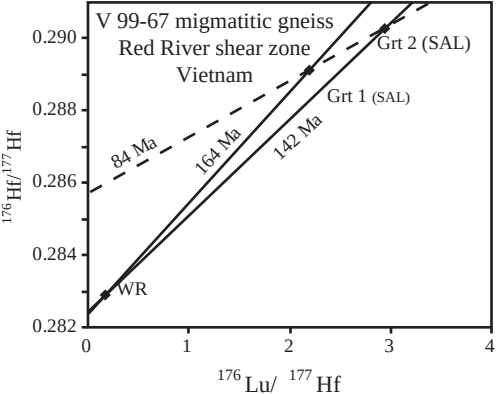

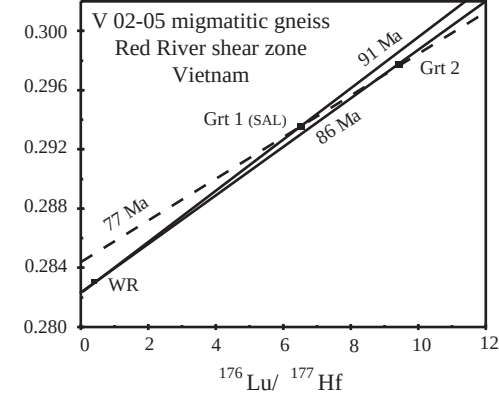

Fig. 7. Lu-Hf isochron diagrams.

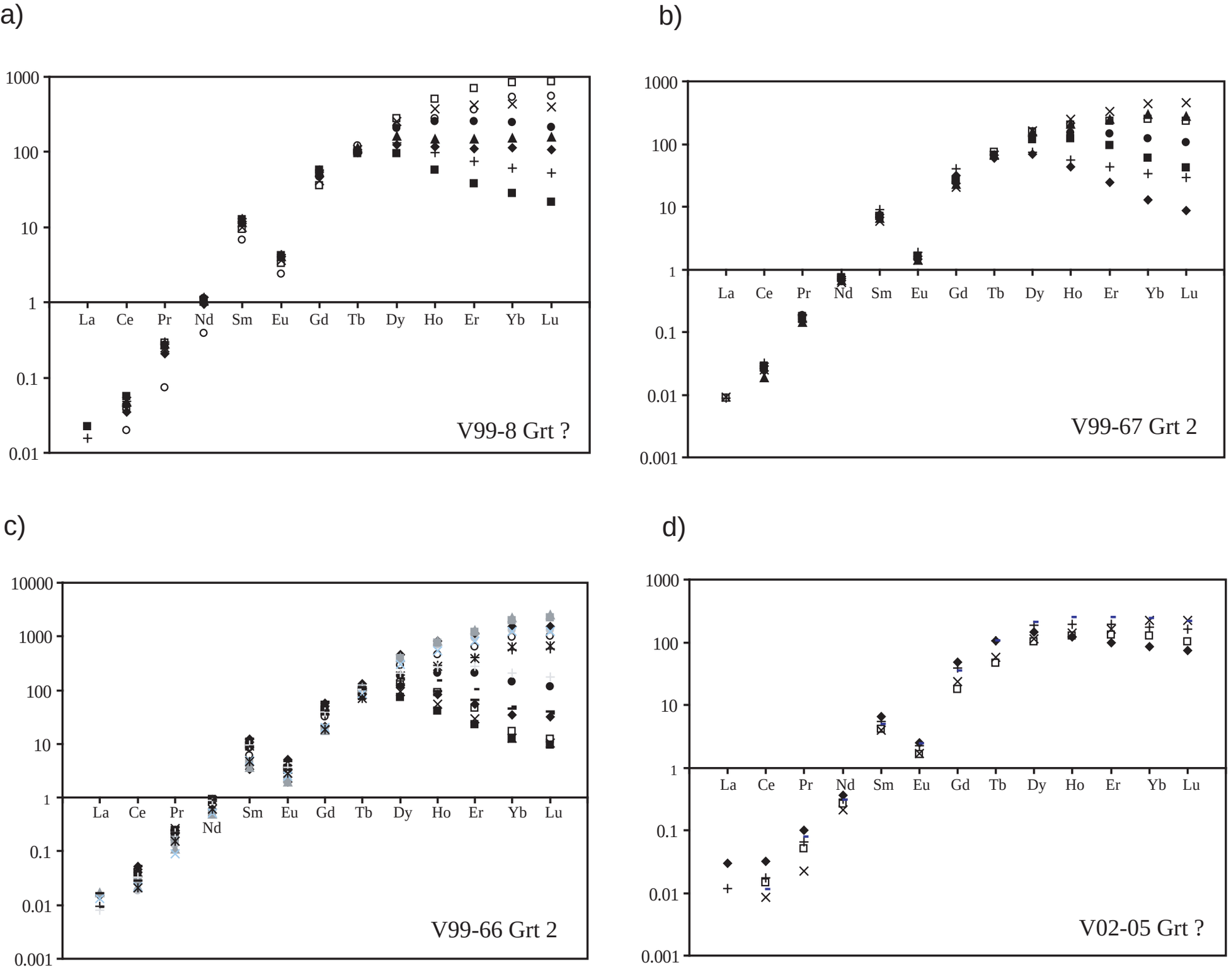

Fig. 8. Represnetative rim-to-rim chondrite normalised Rare Earth Elements plots of garnets.

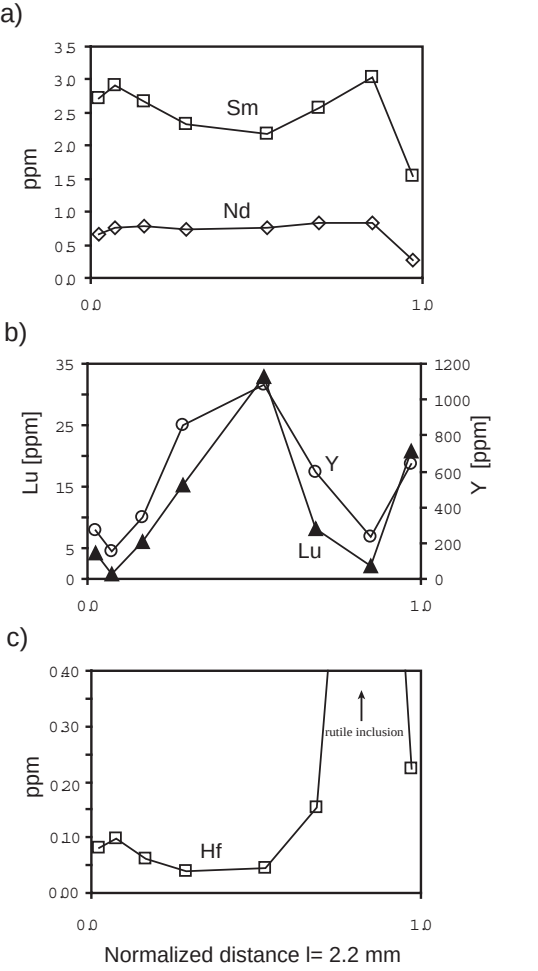

Fig. 9. Rim-to-rim zonation profiles of trace elements in garnets from sample V99-8.

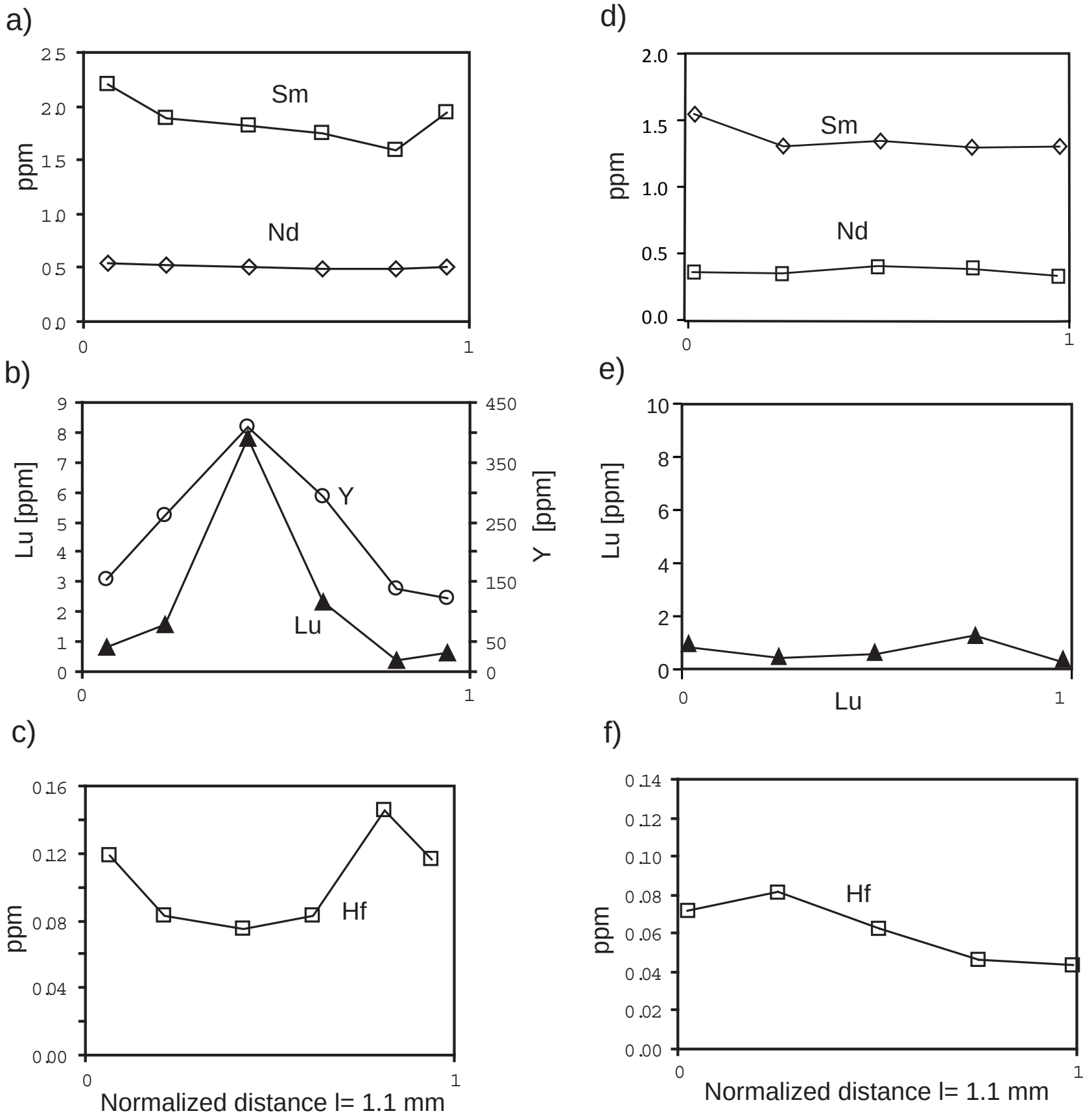

Fig. 10. Rim-to-rim zonation profiles of two garnet crystsls from sample V99-67: Sm and Nd (a, d), Y and Lu (b, e) and Hf (c, f).

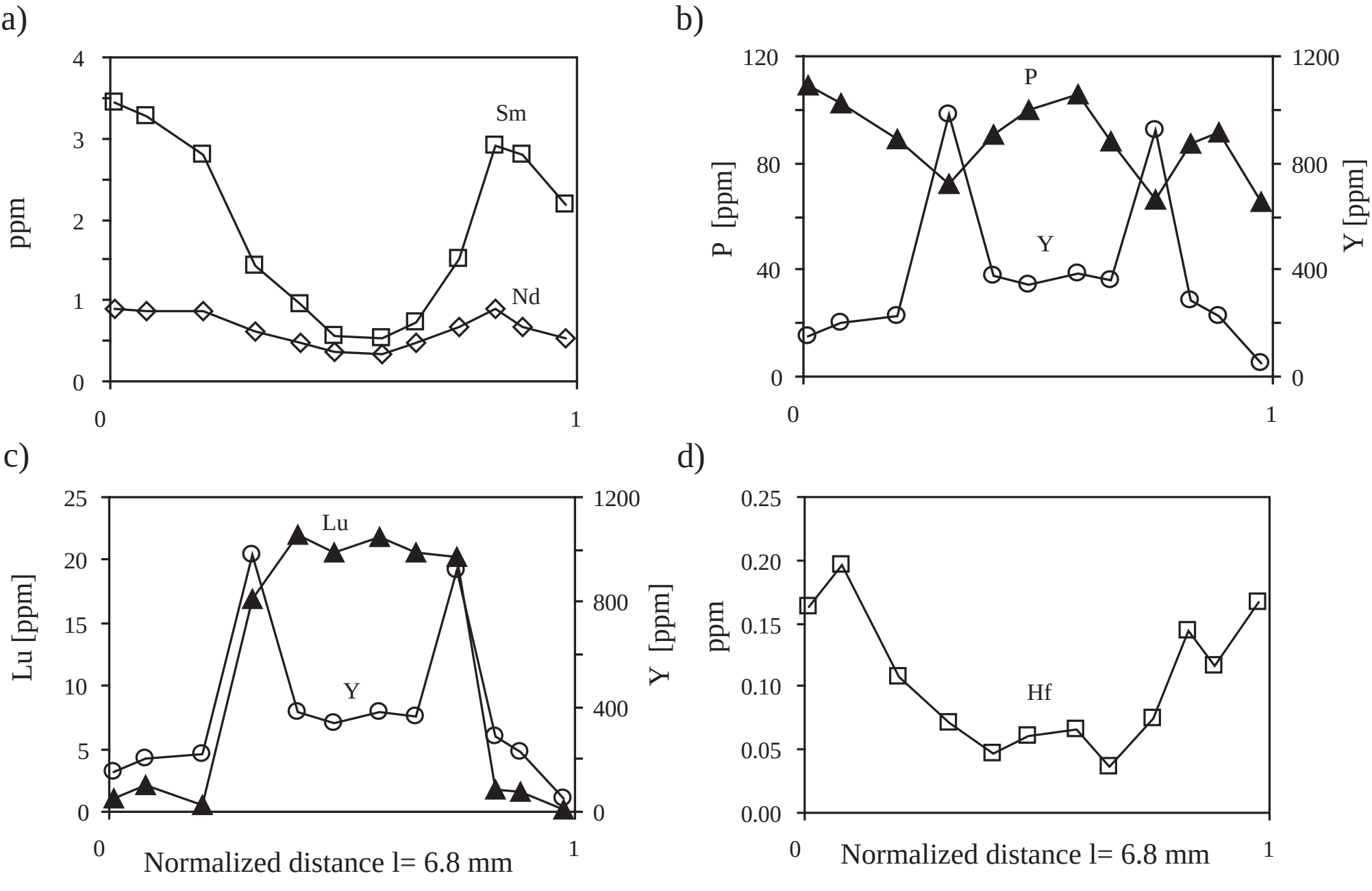

Fig. 11. Rim-to-rim zonation profiles in garnet Grt. 1 from sample V99-66.

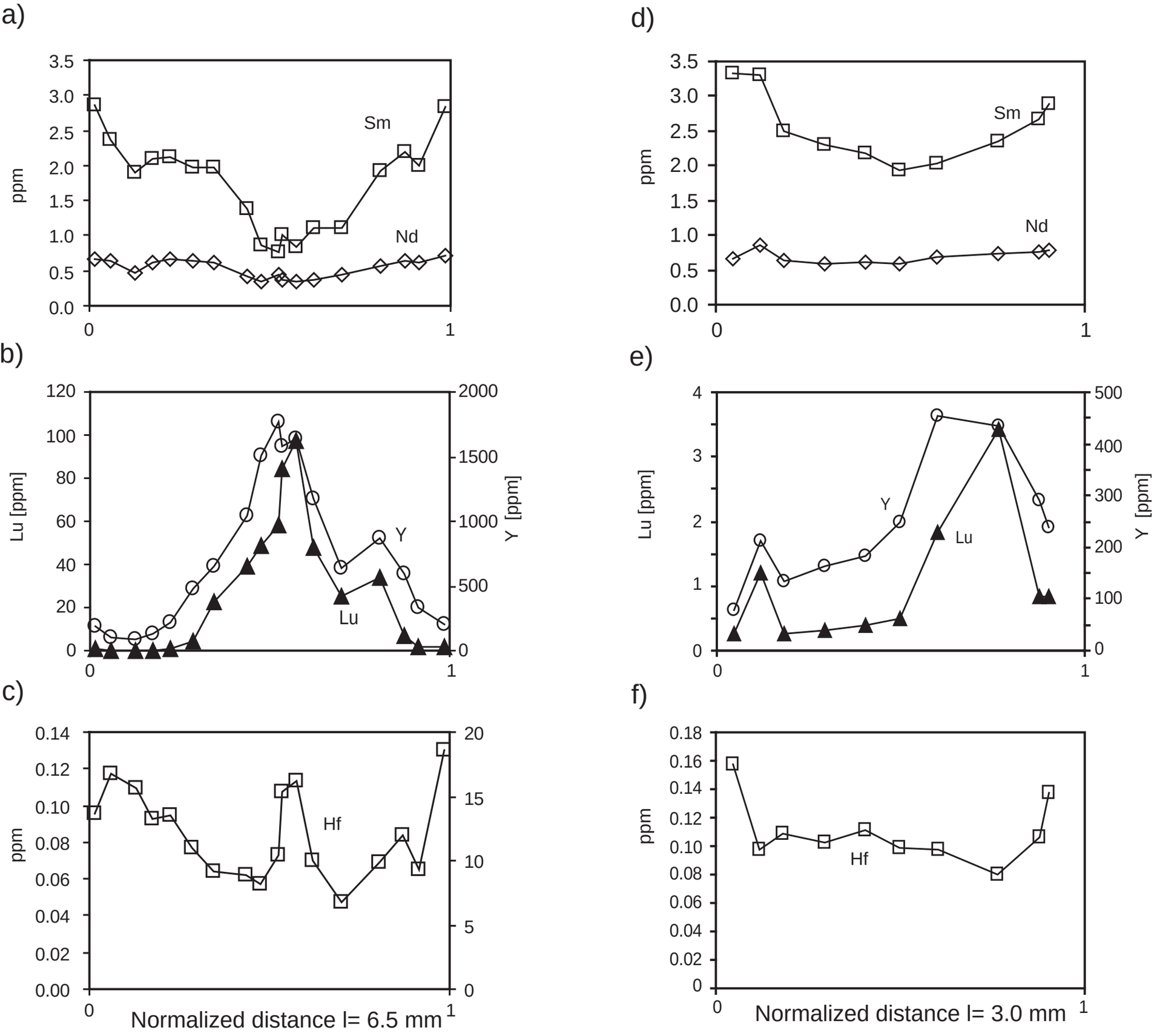

Fig. 12. Rim-to-rim trace element zonation profiles of Grt. 2 (a-c) and Grt. 3 (d-f) from sample V99-66.

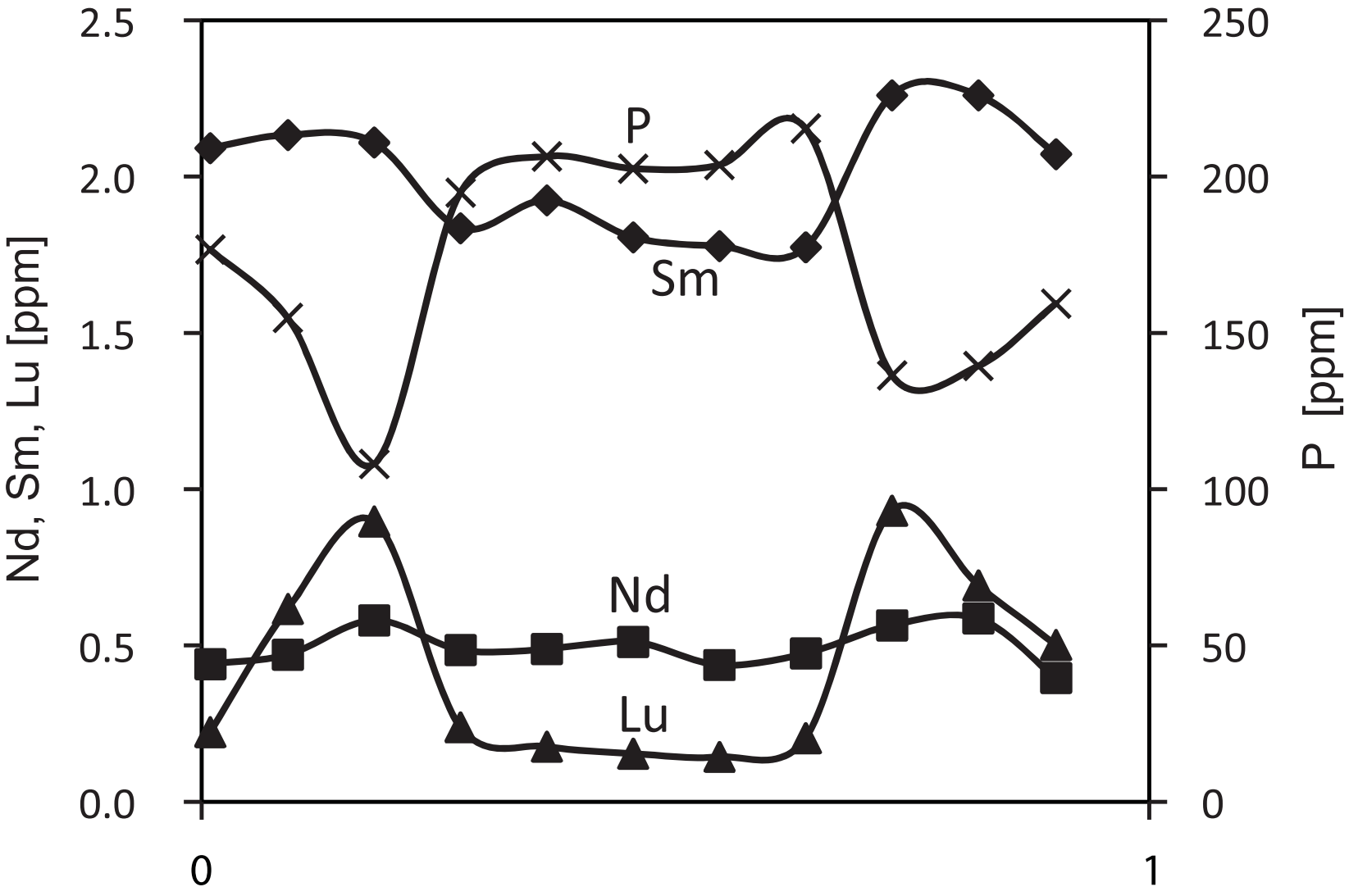
2.5
2.0
1.5
1.0
0.5
0.0
Nd, Sm, Lu [ppm]
250
200
150
100
50
0
P [ppm]
P
Sm
Nd
Lu
0
1

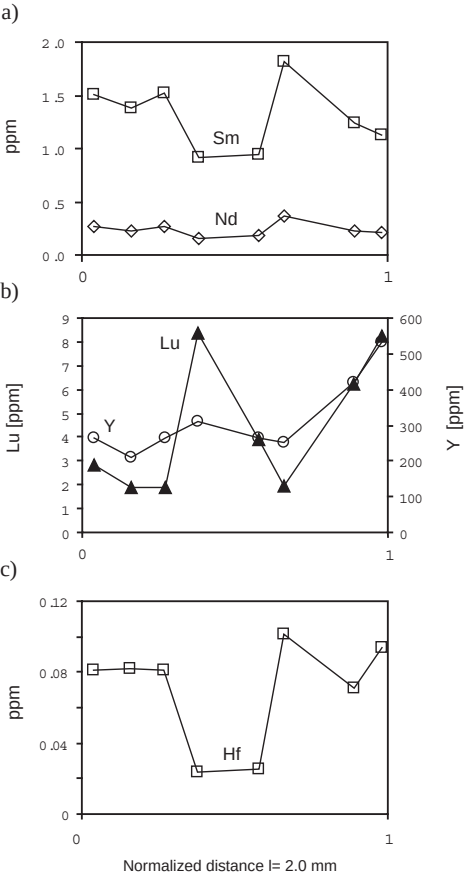

Fig. 13. Rim-to-rim trace element zonation profiles in garnet from sample V02-05.

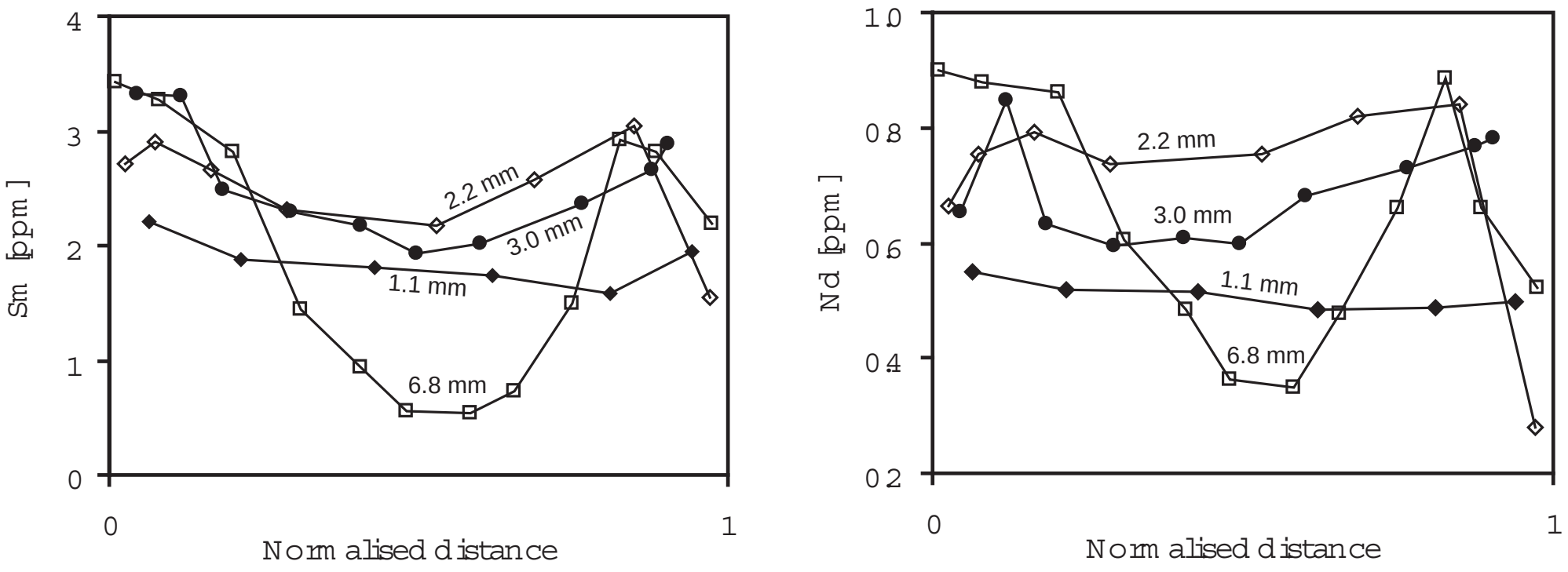

Fig. 14 Nd and Sm rim-to-rim zonation profiles of garnets in dependence on their size.

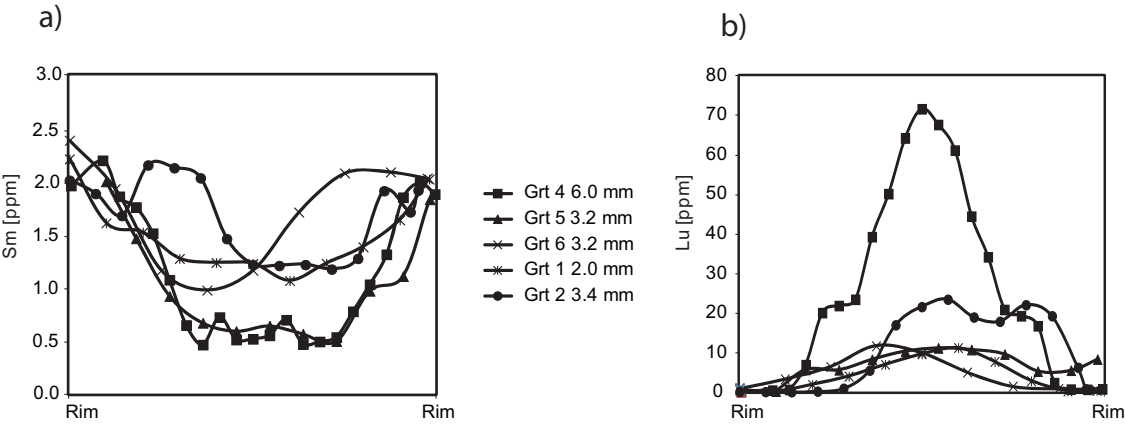
a)
b)
Sm [ppm]
Lu [ppm]
3.0
2.5
2.0
1.5
1.0
0.5
0.0
80
70
60
50
40
30
20
10
0
Rim
Rim
Rim
Rim
Grt 4 6.0 mm
Grt 5 3.2 mm
Grt 6 3.2 mm
Grt 1 2.0 mm
Grt 2 3.4 mm

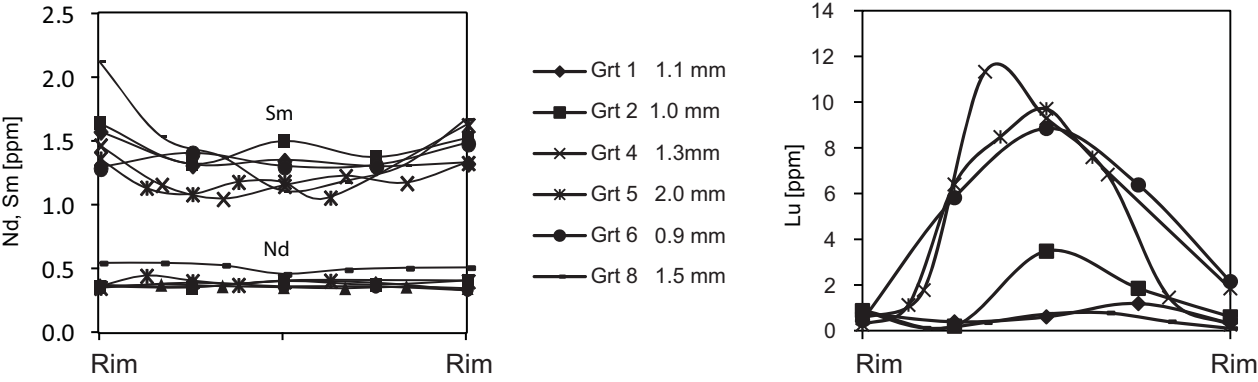
Nd, Sm [ppm]
2.5
2.0
1.5
1.0
0.5
0.0
Sm
Nd
Rim
Rim
Grt 1 1.1 mm
Grt 2 1.0 mm
Grt 4 1.3mm
Grt 5 2.0 mm
Grt 6 0.9 mm
Grt 8 1.5 mm
Lu [ppm]
14
12
10
8
6
4
2
0
Rim
Rim

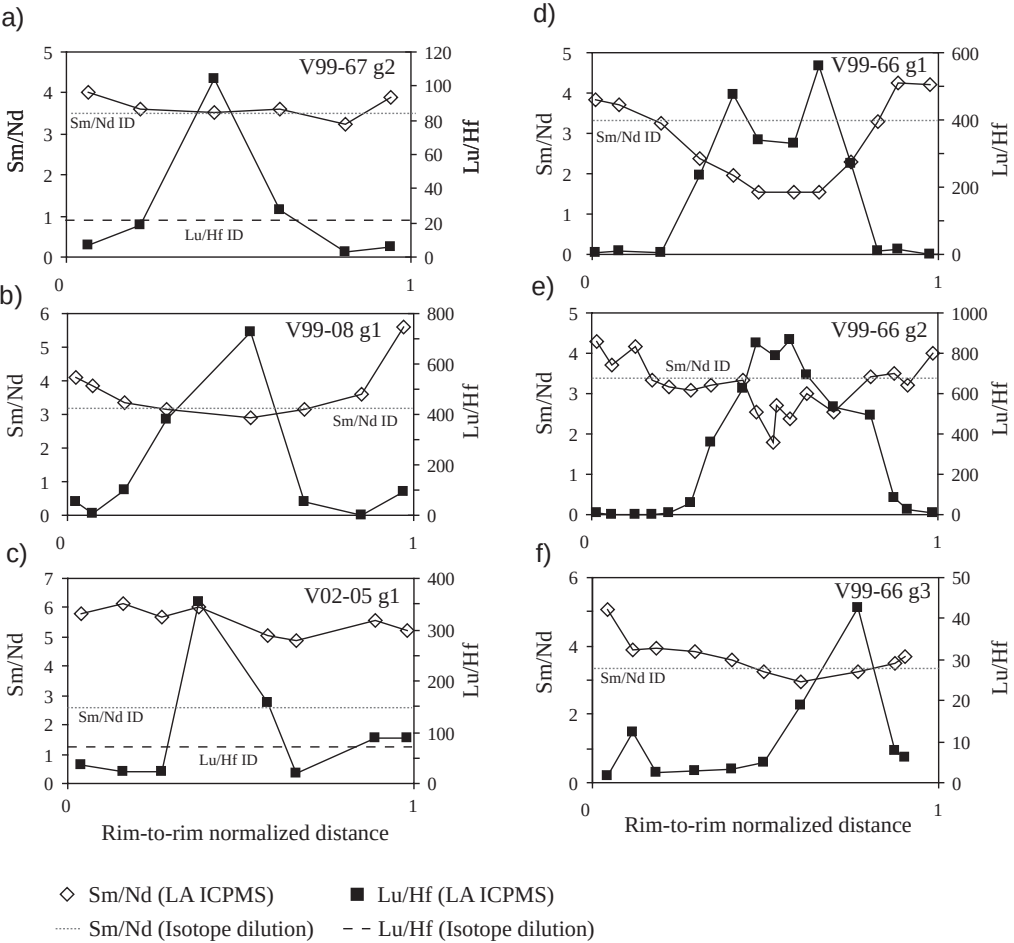

Fig. 16. Rim-to-rim Sm/Nd and Lu/Hf ratios zonation in garnets measured by LA ICPMS.

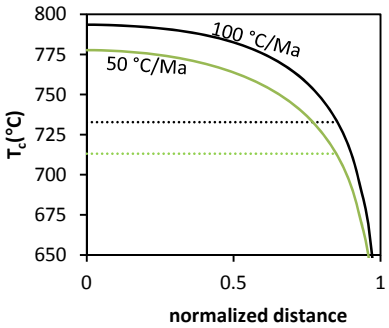

Fig. 15 Nd closure temperature Tc profiles for 1mm diameter garnet for 50 and 100 °C/Ma cooling rates. Dashed lines indicate mean closure temperatures. See text for details.

Table 1. Summary of the Sm-Nd and Lu-Hf dating results.

Label	sample wt [g]	Sm [ppm]	Nd [ppm]	$^{147}Sm/^{144}Nd$	$^{143}Nd/^{144}Nd$	Age [Ma]	Initial $^{143}Nd/^{144}Nd$	ε Nd(t)	Lu [ppm]	Hf [ppm]	$^{176}Lu/^{177}Hf$	$^{176}Hf/^{177}Hf$
99-8 gneiss, Yen Bai area												
WR	0.09683	6.725	34.60	0.1175	0.511787±12	39.1±1.4	0.511757±11	-16.2				
Biot	0.03246	0.221	1.177	0.1135	0.511785±24							
Grt 1	0.03083	1.814	1.016	1.0791	0.512033±14							
Grt 2	0.06601	1.241	0.388	1.9341	0.512252±13							
V99-66 gneiss, Bao Yen area												
WR	0.09915	6.871	35.43	0.1172	0.511776±7	41.4±1.3	0.511742±8	-16.4				
Grt 1 AL step1	0.0168	3.054	1.892	0.9759	0.511987±10							
Grt 1 AL step2	0.00677	3.222	1.808	1.0771	0.512041±20							
Grt 1 AL step3	0.0157	3.381	11.121	0.1838	0.511792±8							
Grt 2 not leached	0.01583	2.295	1.019	1.3617	0.512100±16							
Grt 3 SAL	0.01043	2.999	0.918	1.9739	0.512282±23							
Grt 4 SAL	0.0387	2.064	0.632	1.9730	0.512282±24							
V99-67 gneiss Bao Yen area												
WR 1	0.09525	4.508	21.84	0.1247	0.511956±11	31.7±0.9	0.511930±9	-13.0	0.242	0.209	0.1637	0.282902±19
WR 2		4.503	21.745	0.1252	0.511954±12							
Grt 1	0.04516	3.555	1.222	1.7589	0.512296±13				4.425	0.286	2.1939	0.289120±9
Grt 2	0.04427	3.705	1.051	2.1312	0.512367±11				4.160	0.200	2.9411	0.290293±14
Grt 3		3.661	1.202	1.8406	0.512323±22							
V02-05 Trai Hut area												
WR	0.11268	8.393	41.90	0.1211	0.512059±11	49.8±2.5	0.512015±9	-10.9	0.741	0.2674	0.3921	0.283059±15
Grt 1	0.01239	4.705	18.49	0.1539	0.512061±11				7.568	0.1139	9.4262	0.297700±57
Grt 2 (SAL)	0.02916	1.044	0.409	1.5446	0.512519±22				7.163	0.1553	6.5355	0.293546±28